AD NUMBER

AD-361 711

CLASSIFICATION CHANGES

TO **UNCLASSIFIED**

FROM ~~**CONFIDENTIAL**~~

AUTHORITY

OCA; Apr 30, 1977 IAW Gp-4 Document Marking

19990604253

UNCLASSIFIED

AD NUMBER

AD-361 711

NEW LIMITATION CHANGE

TO DISTRIBUTION STATEMENT - B

Distribution authorized to U.S. Gov't Agencies, only; Specific Authority; 26 May 99. Other requests shall be referred to USAF Special Weapons Center, Kirtland AFB, New Mexico, 87117

LIMITATION CODE: 3

FROM No Prior DoD Distr Scty Cntrl St'mt Assgn'd

AUTHORITY

DoDD 5230.24, para f.3.b.; Apr 30, 1965

THIS PAGE IS UNCLASSIFIED

UNCLASSIFIED [redacted]

GENERAL ATOMIC DIVISION
GENERAL DYNAMICS CORPORATION

John Jay Hopkins Laboratory for Pure and Applied Science
P.O. Box 608, San Diego, California 92112

GAMD-6213
Category A

This document consists of 89 pages
No. 2 of 55 copies, Series A

STABILITY STUDY OF NUCLEAR PULSE PROPULSION (ORION) ENGINE SYSTEM (U)

Work done by:

C. V. David
H. A. Long
F. W. Ross
R. W. Schlicht

Report written by:

C. V. David

This document, which was prepared primarily for internal use at General Atomic, may contain preliminary or incomplete data. It is informal and is subject to revision or correction; it does not, therefore, represent a final report.

Air Force Special Weapons Center
Kirtland Air Force Base, New Mexico
Air Force Systems Command
Contract AF29(601)-6214

Project 372
April 30, 1965

UNCLASSIFIED [redacted]

[redacted]

SECURITY
MARKING

The classified or limited status of this report applies to each page, unless otherwise marked.
Separate page printouts MUST be marked accordingly.

"This document contains information affecting the National Defense of the United States within the meaning of the Espionage Laws, Title 18, U. S. C., Section 793 and 794. Its transmission or the revelation of its contents in any manner to an unauthorized person is prohibited by law."

DOWNGRADED AT 3 YEAR INTERVALS:
DECLASSIFIED AFTER 12 YEARS
DOD DIR 5200.10

" ONE HALF ORIGINAL SIZE " attachment A

[redacted]

UNCLASSIFIED [redacted]

DDC Availability Notice

U.S. Government agencies may obtain copies of this report directly from DDC. Other qualified DDC users shall request through

Contracting Officer
Air Force Special Weapons Center
Kirtland Air Force Base, New Mexico 87117

UNCLASSIFIED [redacted]

[redacted]

UNCLASSIFIED

ABSTRACT

The stability of the nuclear pulse vehicle is defined by the following criterion. If, after a large number of sequenced impulses are delivered to the engine, the lateral and tilting oscillations of the pusher plate and/or the intermediate platform do not build up above a level compatible with a stable operation of the system (i.e., no divergence is present), the stability is ensured. A 10-m-diam engine configuration was investigated to determine whether this requirement was fulfilled when the motions were restricted to one plane, which is actually more severe than three-dimensional motions and therefore conservative.

The basic equations of motion are derived. The restoring spring forces and moments are given. The problem was simulated on an analog computer, for which the computer programs are presented. Typical results obtained with an optimized 10-m-diam engine configuration are also given.

The influence of some of the most important parameters on the system stability was determined. It appears from a preliminary study limited to single-impulse applications that the ORION engine could be made dynamically stable.

UNCLASS

[redacted]

[redacted]LASSIFIED

CONTENTS

UNCLASS...

[redacted]

I. INTRODUCTION

The nuclear-pulse propulsion engine has been described in detail in many reports.[1,2,3] Its operation is very straightforward: the impulse delivered to a plate by an expanding plasma (propellant) generated by a nuclear device explosion is transmitted to the vehicle through a shock-absorbing system that is essentially nondissipative. The explosions are repeated at a fixed time interval to synchronize the oscillating motion of the plate with respect to the vehicle so that a stable "punching ball" phenomenon develops after the first impulse. The stability of the on-axis motion is ensured by the shock-absorber—explosion timing synchronization.[3,4] But if all impulses are not delivered to the plate exactly on axis, a sidewise and/or a tilting motion of the plate will develop. According to the magnitude of the off-centering of the impulse, the damping imposed by the shock-absorber system on these oscillations, their frequencies, etc., an amplitude build-up could occur and that would render the operation of the system unstable. The nature of the problem is also such that the engine configuration influences the over-all vehicle tilting motion and introduces a damping effect which may be positive or negative,[5] depending on the engine configuration adopted.

The present engine configuration consists of three masses connected by two nonlinear springs. Each spring is flexible in all directions and each mass then has six degrees of freedom.[2,4] But practically, the rotation around the engine axis can be ignored since there is no forcing function that could induce this type of oscillation, if the lateral reactions due to the shear forces in the propellant stagnating layer are ignored. Also, if it can be proven that the system is stable in the x-y plane, it is assumed that it will be stable in the x-y-z space.

This is quite obvious since the off-centering of all the impulses is then systematically concentrated in one plane, which increases the frequency at which a given magnitude of off-centering occurs. This approach is therefore conservative.

The simulation of the ORION engine operation on an analog computer was performed to determine whether the system was stable.

II. DERIVATION OF EQUATIONS

A simplified sketch of the over-all system is shown in Fig. 1, where the definition of axes of reference is indicated. All linear and angular displacements are with respect to a fixed frame of reference. Its location is unimportant since all displacements and velocities are treated as differences within the equations. For sake of simplification, the upper mass (M_3) was used as reference.

2.1. EQUATIONS OF MOTION

Each mass, M_1, M_2, and M_3, can move on axis laterally and rotate around its own center of gravity in the x-y plane.

Therefore, the inertial forces of each mass balance the external forces applied to it and one has
for Mass 1, (M_1, I_1),

$$M_1 \frac{d^2 y_1}{dt^2} + \sum F_{y_1} = 0, \tag{1}$$

$$M_1 \frac{d^2 x_1}{dt^2} + \sum F_{x_1} = 0, \tag{2}$$

$$I_1 \frac{d^2 \theta_1}{dt^2} + \sum M_{\theta_1} = 0; \tag{3}$$

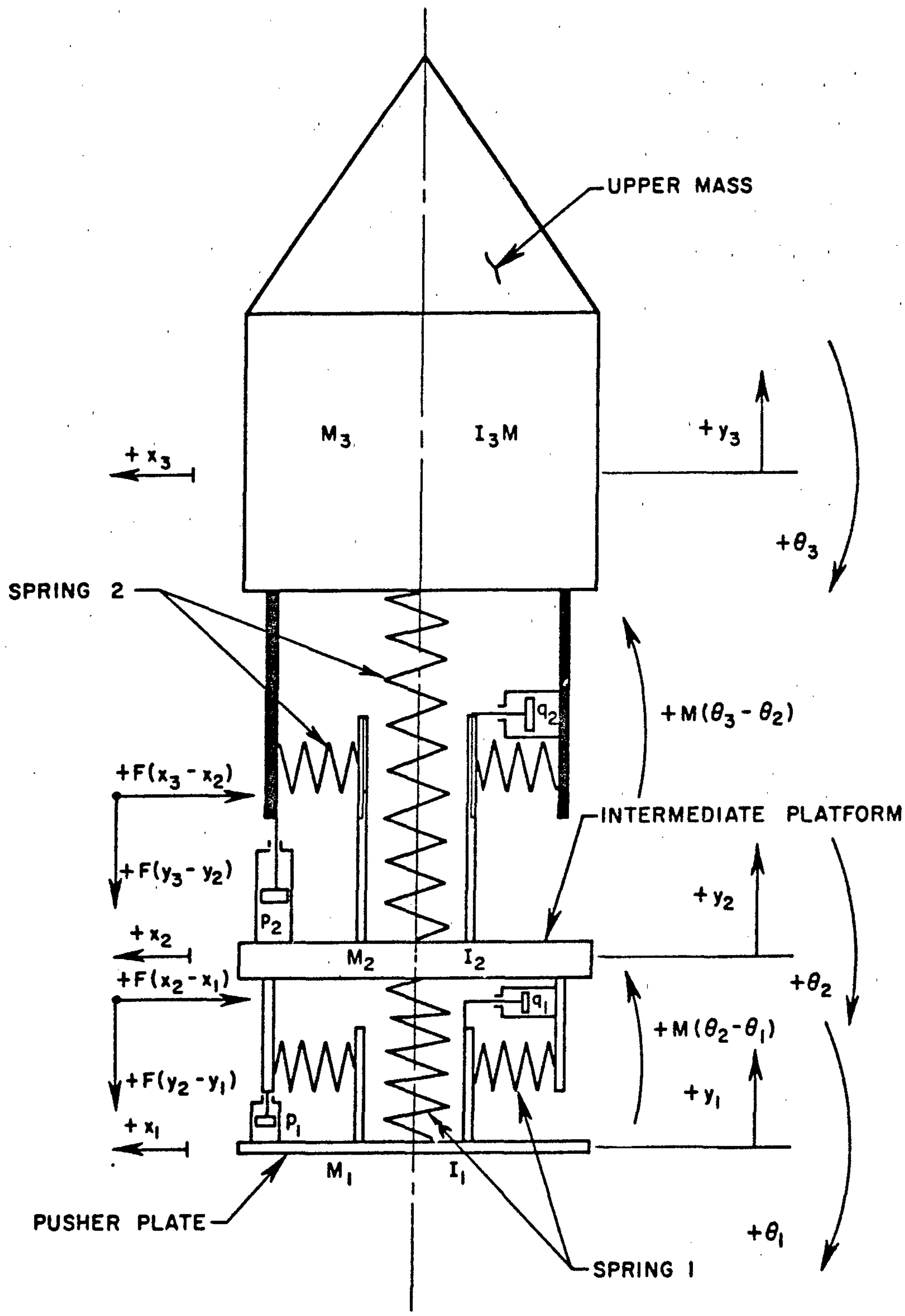

Fig. 1--ORION vehicle schematic

for Mass 2, (M_2, I_2),

$$M_2 \frac{d^2 y_2}{dt^2} + \sum F_{y_2} = 0, \tag{4}$$

$$M_2 \frac{d^2 x_2}{dt^2} + \sum F_{x_2} = 0, \tag{5}$$

$$I_2 \frac{d^2 \theta_2}{dt^2} + \sum M_{\theta_2} = 0; \tag{6}$$

for Mass 3, (M_3, I_3),

$$M_3 \frac{d^2 y_3}{dt^2} + \sum F_{y_3} = 0, \tag{7}$$

$$M_3 \frac{d^2 x_3}{dt^2} + \sum F_{x_3} = 0, \tag{8}$$

$$I_3 \frac{d^2 x_3}{dt^2} + \sum M_{\theta_3} = 0. \tag{9}$$

The springs are assumed to have no mass, but their actual masses are included in M_1 and M_2. All F_y and F_x forces are the sum of the spring elastic forces and damping reactions. The same applies to the moments.

The on-axis spring elastic forces derived as given in Ref. 4, are:

Spring 1

$$F(y_2 - y_1) = A \left[5.5 \frac{(y_{2,00} - y_{1,00}) - (y_2 - y_1)}{(y_{2,00} - y_{1,00})} - 165 \left\{ \frac{(y_{2,00} - y_{1,00}) - (y_2 - y_1)}{(y_{2,00} - y_{1,00})} \right\}^4 \right]$$

$$\text{for } y_2 - y_1 > y_{2,00} - y_{1,00}, \tag{10}$$

and

$$F(y_2-y_1) = A \left[4 \frac{(y_{2,00} - y_{1,00}) - (y_2 - y_1)}{(y_{2,00} - y_{1,00})} + 5.7 \left\{ \frac{(y_{2,00} - y_{1,00}) - (y_2 - y_1)}{(y_{2,00} - y_{1,00})} \right\}^2 \right]$$

$$\text{for } y_2 - y_1 \leq y_{2,00} - y_{1,00}. \quad (11)$$

Spring 2

$$F(y_3-y_2) = \left(\frac{B}{S} + C\right)\left[(y_{3,00} - y_{2,00}) - (y_3 - y_2)\right]$$

$$\text{for } - S < \left[(y_{3,00} - y_{2,00}) - (y_3 - y_2)\right] < + S, \quad (12)$$

$$F(y_3-y_2) = B + C \left[(y_{3,00} - y_{2,00}) - (y_3 - y_2)\right]$$

$$\text{for } \left[(y_{3,00} - y_{2,00}) - (y_3 - y_2)\right] \geq S, \quad (13)$$

$$F(y_3-y_2) = -B + C \left[(y_{3,00} - y_{2,00}) - (y_3 - y_2)\right]$$

$$\text{for } \left[(y_{3,00} - y_{2,00}) - (y_3 - y_2)\right] \leq - S. \quad (14)$$

In these equations, A, B, C, and S are coefficients used to adjust the system frequency to ensure the system synchronization in the axial mode.[4]

Viscous damping is assumed and made adjustable to simulate exactly the total amount of damping expected in the spring, as calculated in Ref. 4. Then one has for Spring (1)

$$p_1 \left(\frac{dy_1}{dt} - \frac{dy_2}{dt}\right) \quad (15)$$

$$r_1 \left(\frac{dx_1}{dt} - \frac{dx_2}{dt}\right) \quad (16)$$

and for Spring (2)

$$p_2 \left(\frac{dy_2}{dt} - \frac{dy_3}{dt}\right) \tag{17}$$

$$r_2 \left(\frac{dx_2}{dt} - \frac{dx_3}{dt}\right) \tag{18}$$

The lateral forces developed by the two springs, as calculated from equations derived in Ref. 6, are

<u>Spring (1)</u>

$$F(x_2-x_1) = (x_1 - x_2)\left[k_1' \left(\frac{D_1}{x_1^*} + \frac{D_2}{x_2^*}\right) + k_1'' \left(\frac{D_3}{x_3^*} + \frac{D_4}{x_4^*} + \frac{D_5}{x_5^*}\right)\right], \tag{19}$$

where k_1' and k_1'' are computed constants determined by the spring configuration and D_1 to D_5 are the torus stack diameters; x_1^*, ···, x_5^* are lateral rigidity coefficients given by

$$x_i^* = \frac{4}{3\pi\, K_{nx}\, f(\frac{\Delta y}{d})} \left\{\lambda_i \left(1 - \frac{\Delta y}{d}\right)\left[3\mu_i + 2\lambda_i \left(1 - \frac{\Delta y}{d}\right)\right]\right\}$$

$$+ \frac{\sigma_0}{E \sin\beta_0 \sin\beta \cos\beta}, \tag{20}$$

where

$$\lambda_i = \frac{y_{2,00} - y_{1,00}}{D_i},$$

$$\mu_i = \frac{M(\theta_2 - \theta_1)_i}{D_i\, F(x_2 - x_1)_i},$$

$$\frac{\Delta y}{d} = \frac{(y_{2,00} - y_{1,00}) - (y_2 - y_1)}{(y_{2,00} - y_{1,00})}.$$

$M(\Theta_2-\Theta_1)_i$ is defined later (see Eq. 28), β_0, σ_0, and E are given constants; β_0 is the half-angle made by the filaments of the torus wall structure in the neutral position, σ_0 and E_0 are filament material mechanical characteristics[6]; K_{nx}, β, and $f(\frac{\Delta y}{d})$ are defined as follows

For $(y_{2,00} - y_{1,00}) - (y_2 - y_1) > 0$

$K_{nx} = \frac{dN_x}{d(\Delta y)}$ with $N_x = \frac{\pi}{2}\Delta y$, since the value of $\beta = \beta_0$ was assumed more realistic here[6] ($\beta = \beta_0 = 35.3$ degrees) and

$$f(\frac{\Delta y}{d}) = \left[\frac{1}{1 - (\frac{\Delta y}{d})^2}\right]^{1.3} \tag{21}$$

for a polytropic compression (or expansion) characterized by $\gamma = 1.3$.

For $(y_{2,00} - y_{1,00}) - (y_2 - y_1) < 0$

Here, only the case of β variable is considered (see Ref. 6 for the justification). Then,

$$N_x = \frac{\cos a_0}{\sin a_0 - \frac{2a_0}{\pi}\frac{\cos \beta_0}{\cos \beta}}\Delta y, \tag{22}$$

where a_0 is defined by the equation[6]

$$\sin a_0 = \frac{2a_0}{\pi}\left(1 + \frac{\Delta y}{d}\right), \tag{23}$$

$$\beta = \tan^{-1}\sqrt{\frac{1}{2}\left(1 - \frac{\sin a_0 \cos a_0}{a_0}\right)}, \tag{24}$$

$$f\left(\frac{\Delta y}{d}\right) = \left[\frac{2a_0}{\pi\left(1 - \frac{\sin 2a_0}{2a_0}\right)}\right]^{1.3} . \qquad (25)$$

Spring (2)

This spring operates essentially as a constant section beam in bending but of variable length, and

$$F(x_3 - x_2) = K_3 \left\{L_0 - \left[(y_{3,00} - y_{2,00}) - (y_3 - y_2)\right]\right\}^{-3} (x_2 - x_3 \pm t), \quad (26)$$

where K_3 is a constant (see Appendix A for the derivation), L_0 is the characteristic length of the second spring in the neutral position, and t is used as follows: If

$$-t < x_2 - x_3 < +t,$$

then

$$F(x_3 - x_2) = 0$$

since there is no restoring side force. If $x_2 - x_3 > +t$, then $-t$ is used in Eq. (26); if $x_2 - x_3 < -t$, then $+t$ is used in Eq. (26). t represents the backlash effect caused by the clearance existing between the piston stem and the guiding cylinder (see Refs. 4 and 7), and, finally, as an approximation

$$t = t_1 \frac{\lambda_0 - [(y_{3,00} - y_{2,00}) - (y_3 - y_2)]}{\lambda_0 + [(y_{3,00} - y_{2,00}) - (y_3 - y_2)]} \qquad (27)$$

where t_1 is the clearance defined above and λ_0 is a function of the nominal stroke of the second spring and is used as an adjustable constant to simulate the effect of the backlash, defined above, on the lateral displacement of the intermediate platform.

The restoring moment for spring (1) is derived in Ref. 6 and is

$$M(\theta_2-\theta_1) = (\theta_1 - \theta_2)\left[k_1'\left(\frac{D_1^3}{\theta_1^*} + \frac{D_2^3}{\theta_1^*}\right) + k_1''\left(\frac{D_3^3}{\theta_3^*} + \frac{D_4^3}{\theta_4^*} + \frac{D_5^3}{\theta_5^*}\right)\right], \tag{28}$$

and θ_i^* is given as

$$\theta_i^* = \frac{4}{\pi K_{nx} f\left(\frac{\Delta y}{d}\right)}\left[2 + \frac{\lambda_i}{\mu_i}\left(1 - \frac{\Delta y}{d}\right)\right] \tag{29}$$

To compute μ_i, $M(\theta_2-\theta_1)_i$ and $F(x_2-x_1)_i$ must be calculated for each torus stack; this is included in the program for simulation with the analog computer and it characterizes the cross-coupling between the lateral- and tilting-motion modes.

The restoring moment for spring (2) is simply

$$M(\theta_3-\theta_2) = K_2 \tan \Delta\theta \{L_0 - [(y_{3,00} - y_{2,00}) - (y_3 - y_2)]\}^{-1} \tag{30}$$

where

$$\Delta\theta = (\theta_2 - \theta_3) - \frac{2(x_2 - x_3)}{L_0 - [(y_{3,00} - y_{2,00}) - (y_3 - y_2)]}$$

and K_2 is a constant calculated from the shock-absorber design data (see Appendix B). The effect of the second mass lateral displacement on the second spring restoring moment is thus included.

The damping of this motion mode is also assumed to be viscous in nature and can be expressed as

$$q_1 \left(\frac{d\theta_1}{dt} - \frac{d\theta_2}{dt}\right) \text{ for spring (1),}$$

$$q_2 \left(\frac{d\theta_2}{dt} - \frac{d\theta_3}{dt}\right) \text{ for spring (2).}$$

The substitution of all elastic forces and viscous forces in their respective equations then yields the nine basic equations of motions for the masses:

$$M_1 \frac{d^2y_1}{dt^2} + F(y_2-y_1) + p_1\left(\frac{dy_1}{dt} - \frac{dy_2}{dt}\right) = 0, \tag{31}$$

$$M_2 \frac{d^2y_2}{dt^2} - F(y_2-y_1) + F(y_3-y_2) - p_1\left(\frac{dy_1}{dt} - \frac{dy_2}{dt}\right) + p_2\left(\frac{dy_2}{dt} - \frac{dy_3}{dt}\right) = 0, \tag{32}$$

$$M_3 \frac{d^2y_3}{dt^2} - F(y_3-y_2) - p_2\left(\frac{dy_2}{dt} - \frac{dy_3}{dt}\right) = 0, \tag{33}$$

$$I_1 \frac{d^2\theta_1}{dt^2} + M(\theta_2-\theta_1) + q_1\left(\frac{d\theta_1}{dt} - \frac{d\theta_2}{dt}\right) = 0, \tag{34}$$

$$I_2 \frac{d^2\theta_2}{dt^2} - M(\theta_2-\theta_1) + M(\theta_3-\theta_2) - q_1\left(\frac{d\theta_1}{dt} - \frac{d\theta_2}{dt}\right) + q_2\left(\frac{d\theta_2}{dt} - \frac{d\theta_3}{dt}\right) = 0, \tag{35}$$

$$I_3 \frac{d^2\theta_3}{dt^2} - M(\theta_3-\theta_2) - q_2\left(\frac{d\theta_2}{dt} - \frac{d\theta_3}{dt}\right) = 0, \tag{36}$$

$$M_1 \frac{d^2x_2}{dt^2} + F(x_2-x_1) + r_1\left(\frac{dx_1}{dt} - \frac{dx_2}{dt}\right) = 0, \tag{37}$$

$$M_2 \frac{d^2x_2}{dt^2} - F(x_2-x_1) + F(x_3-x_2) - r_1\left(\frac{dx_1}{dt} - \frac{dx_2}{dt}\right) + r_2\left(\frac{dx_2}{dt} - \frac{dx_3}{dt}\right) = 0, \quad (38)$$

$$M_3 \frac{d^2x_3}{dt^2} - F(x_3-x_2) - r_2\left(\frac{dx_2}{dt} - \frac{dx_3}{dt}\right) = 0. \quad (39)$$

2.2. SYSTEM-OPERATION EQUATIONS

The system is started by giving a half-nominal impulse to mass M_1 and subsequently a full impulse, I_0, which is defined by either a vehicle velocity increment, ΔV_t, or a plate velocity increment, ΔV_p, per cycle.[2,3] This full impulse is delivered to M_1 when the latter reaches its neutral position during the return stroke if certain conditions are fulfilled. These are given later in this section.

Then,

$$\Delta V_p = \frac{I_0}{M_1} = 2\left(\frac{dy_1}{dt}\right)_e = \frac{\Delta V_t \ (M_1 + M_2 + M_3)}{M_1}. \quad (40)$$

To start the operation, only $(dy_1/dt)_e$ is imposed on M_1, but subsequently $2(dy_1/dt)_e$ is used. This means that if M_1 reaches its neutral position at a time t, at time $t - \delta t$, the velocity of M_1 is $(dy_1/dt)_{t-\delta t}$ and at time $t + \delta t$ it must be

$$\left(\frac{dy_1}{dt}\right)_{t+\delta t} = \left(\frac{dy_1}{dt}\right)_{t-\delta t} + 2\left(\frac{dy_1}{dt}\right)_e \quad (41)$$

if one assumes that during the time interval $2\ \delta t$ the whole impulse $2(dy_1/dt)_e$ is delivered to M_1. Since the value of dy_1/dt is known at all times, the initial conditions of each new cycle are then well defined for the on-axis displacement.

The value of $2(dy_1/dt)_e$ is not constant; it varies around a nominal value at random according to a gaussian distribution based on an evaluation of the energy release variation from one explosion to the other (variable yield) and on an evaluation of the influence of the explosion standoff distance, which affects the momentum delivered to the vehicle.[3] A realistic impulse distribution curve is given in Fig. 2, and corresponds to an asymmetrical nuclear charge yield distribution as shown in the corner of Fig. 2. At some time prior to t, a value of $(dy_1/dt)_e$ is chosen by a program subroutine and stored until it is delivered if the three mass positions and velocities are deemed adequate, as defined later. If so, according to the amount of off-centering of the explosion and the tilting of mass M_1, a lateral impulse and an angular impulse are also delivered to M_1 proportionally to $(dy_1/dt)_e$ such that

$$\left(\frac{d\Theta_1}{dt}\right)_e = \frac{2}{r_g^2}\left(\frac{dy_1}{dt}\right)_e \cdot f(\Delta x), \tag{42}$$

$$\left(\frac{dx_1}{dt}\right)_e = 2\left(\frac{dy_1}{dt}\right)_e \cdot f(\Delta\Theta) \tag{43}$$

if r_g is mass M_1 radius of gyration; $f(\Delta x)$ and $f(\Delta\Theta)$ are functions of the off-centering Δx and of the momentum resultant vector tilting $\Delta\Theta$, respectively.

Therefore, at time $t + \delta t$

$$\left(\frac{d\Theta_1}{dt}\right)_{t+\delta t} = \left(\frac{d\Theta_1}{dt}\right)_{t-\delta t} + \left(\frac{d\Theta_1}{dt}\right)_e , \tag{44}$$

$$\left(\frac{dx_1}{dt}\right)_{t+\delta t} = \left(\frac{dx_1}{dt}\right)_{t-\delta t} + \left(\frac{dx_1}{dt}\right)_e . \tag{45}$$

The value of Δx depends on several variables and conditions. For instance, it is a function of a value Δx_e corresponding to a random distribution of the explosion location (see Fig. 3). It is also a function of the pulse-system delivery system location and of the velocity at the time the pulse system left the gun muzzle. In addition, it is a function

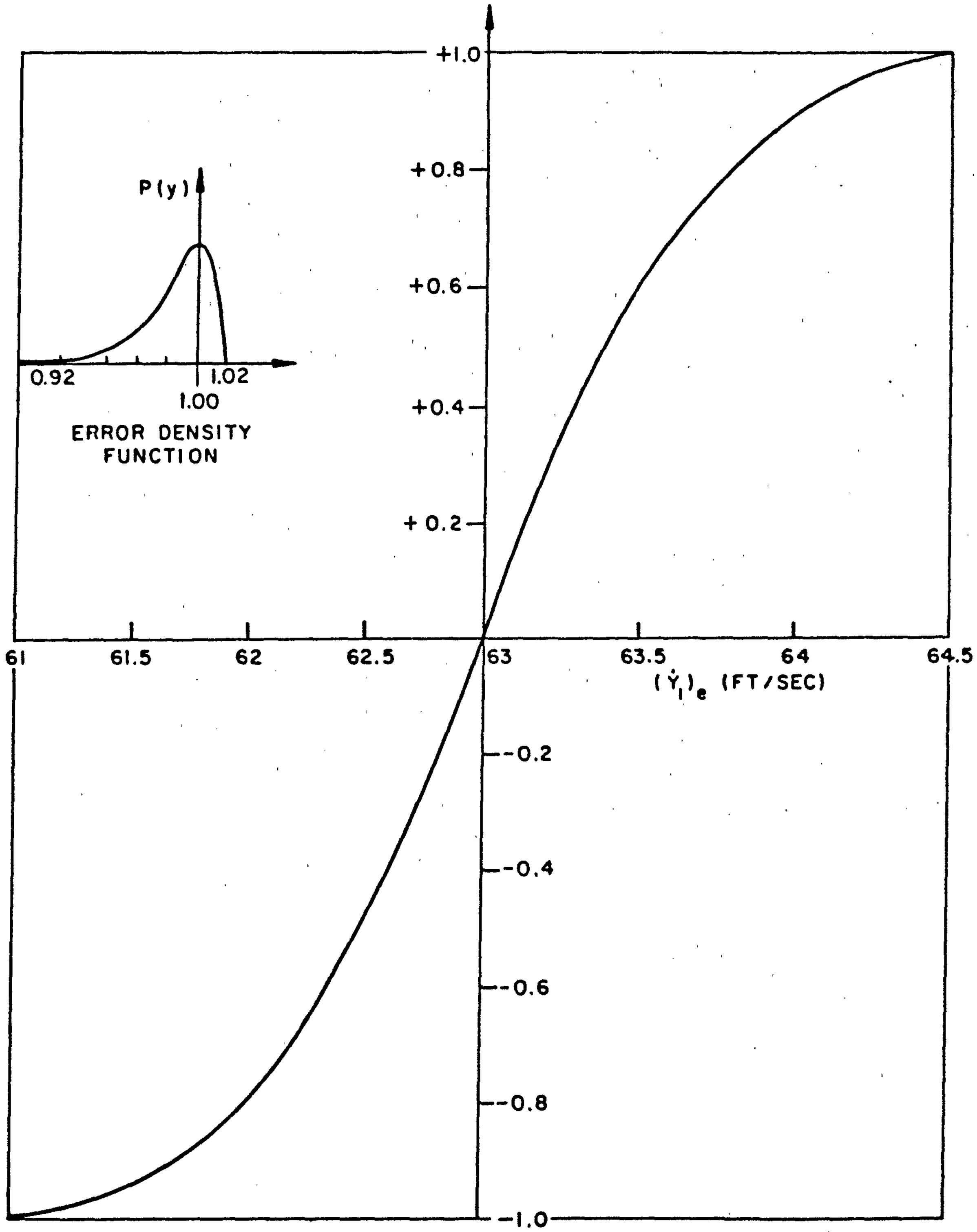

Fig. 2--Impulse error distribution function

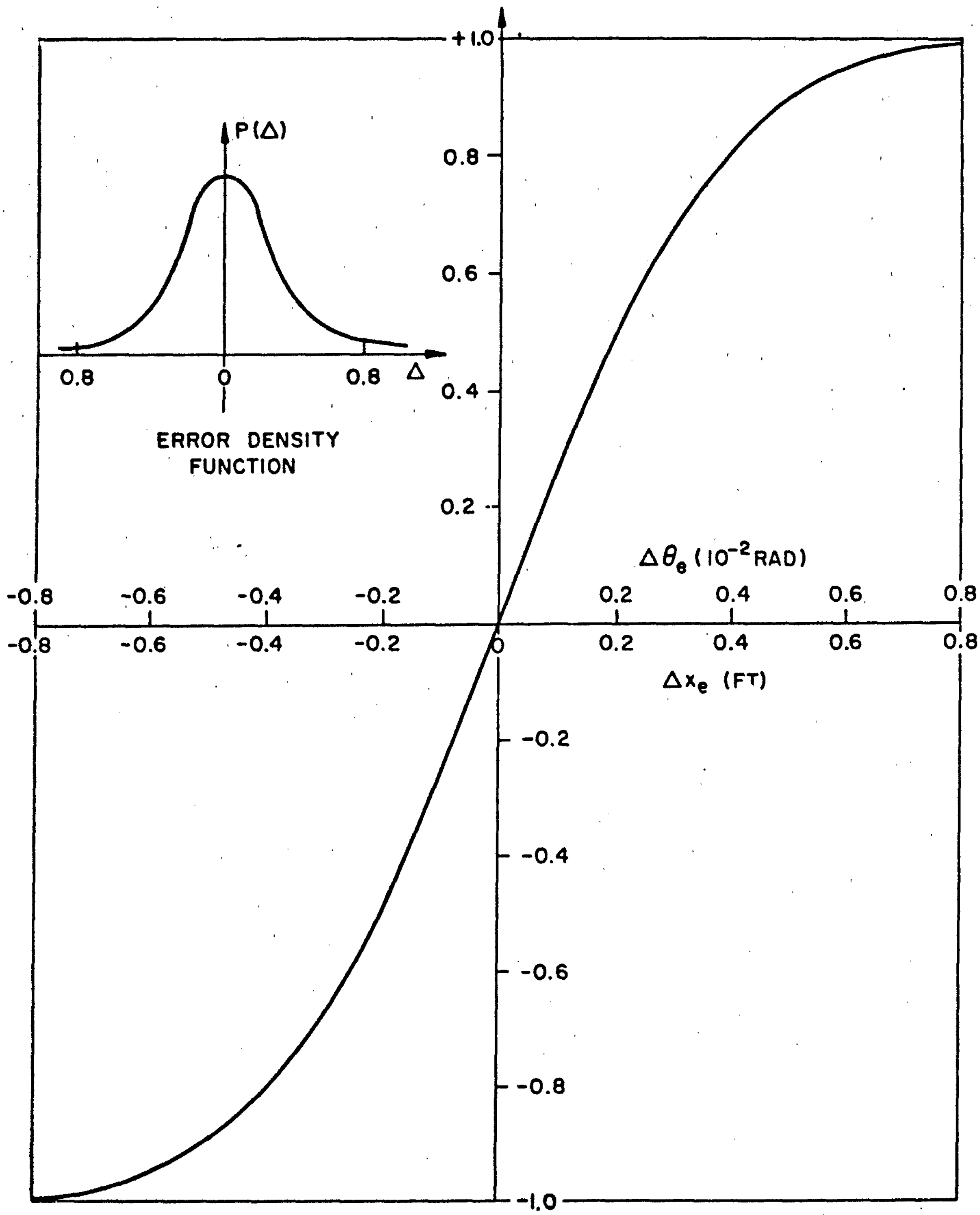

Fig. 3--Pulse system off-centering and misorientation error distribution function

of the position of the plate at the time of the explosion, it was assumed that all those effects were only algebraically additive without any cross-coupling existing between one another and that

$$\Delta x = \Delta x_e + \delta x_1 + \delta x_2 + \delta x_3, \tag{46}$$

where

$$\delta x_1 = - x_1(t) + x_{3(t-\Delta t)} - \left[\left(\frac{dx_1}{dt}\right)_{t-\Delta t} - \left(\frac{dx_3}{dt}\right)_{t-\Delta t}\right]\Delta t - x_{4(t)} \tag{47}$$

if the free flight of the pulse system lasts Δt. δx_1 corresponds to the explosion off-centering caused by the lateral motion of the system. The term $-x_{4(t)}$ corresponds to a correction factor used to cancel any sidewise effect of the over-all center of gravity and

$$x_{4(t)} = \left(\frac{M_1 x_1 + M_2 x_2 + M_3 x_3}{M_1 + M_2 + M_3}\right)_t$$

$$\delta x_2 = \Lambda\left(\frac{d\Theta_3}{dt} - \frac{d\Theta_4}{dt}\right)_{t-\Delta t} \Delta t, \tag{48}$$

where Λ is the distance from the explosion location to the gun muzzle.

δx_2 is the off-centering contribution caused by the angular velocity of the upper vehicle at the time the pulse system left the gun muzzle.

Finally, δx_3, corresponding to the lack of alignment of the gun due to the misorientation of the upper vehicle at time $t-\Delta t$, is

$$\delta x_3 = \left[\Theta_{3(t-\Delta t)} - \Theta_{4(t)}\right] L_1 \Delta t, \tag{49}$$

where L_1 is the distance between the explosion location and the center of gravity of the upper vehicle.

Furthermore, $\Delta\Theta$ is the sum of several individual contributions to the pulse system misorientation, and

$$\Delta\Theta = \delta\Theta_1 + \sum \delta\Theta_i, \tag{50}$$

where $\delta\Theta_i$ is the error caused by a specific subsystem that affects the pulse-system orientation. For instance, the misalignment of the pusher plate causes an error. $\delta\Theta_1 = - \Theta_{1(t)}$ if there are no viscous forces developed in the propellant stagnating against the plate (case of a simple hydrostatic pressure). The evaluation of all $\delta\Theta$'s is quite complex and their influence would be small; therefore, as a first approximation, this influence was neglected; one then has

$$\Delta\Theta = - \Theta_1(t) + \Theta_4(t) \tag{51}$$

The term $\Theta_{4(t)}$ is defined as $\left(\frac{I_1\,\Theta_1 + I_2\,\Theta_2 + I_3\,\Theta_3}{I_1 + I_2 + I_3}\right)_{(t)}$ and is used to readjust the problem after each cycle to avoid the influence of a slow diverging angular drift of the longitudinal axis of the system.

Finally, knowing Δx and $\Delta\Theta$, one can write the expressions of $f(\Delta x)$ and $f(\Delta\Theta)$. Reference 8 gives the cross-coupling relationship between off-centering and misorientation of the pulse system, and one has

$$f(\Delta x) = 0.62\ \Delta x + 0.68 L_2 \Delta\Theta_e, \tag{52}$$

where L_2 is the distance between the explosion and the plate (stand-off distance) and $\Delta\Theta_e$ is the random error of the pulse-system alignment at the time of the explosion. $\Delta\Theta_e$ is given by the curve of Fig. 3, and $f(\Delta\Theta)$ is simply equal to $\Delta\Theta$, as a first approximation.

The problem is now perfectly defined in the ideal case where an impulse is applied to M_1 at the beginning of every cycle. But if, for instance, the impulse chosen from the distribution curve of Fig. 2 is too small or if values of $\Delta\theta_e$ and Δx_e sampled are beyond acceptable limits, the impulse is not delivered (misfire case)[3] and $(dy_1/dt)_e = 0$. For this condition, the plate passes through the neutral position at a velocity $(dy_1/dt)_t$ and is stopped by the two springs operating in tension. The plate then returns through the neutral position and a second compression cycle starts. When the plate returns to its neutral position (end of the second compression half-cycle), the impulse is delivered if all conditions are satisfactory and the normal operation is resumed. If the conditions are not satisfactory (for instance, if there was too much damping present in the system), the axial oscillation of the plate is allowed to damp out and the problem is restarted from rest.

Reference 4 gives the various limits for the displacement and velocity values of mass M_1 and M_2 within which $[(y_{2,00} - y_{1,00}) - (y_2 - y_1)]$, $[(y_{3,00} - y_{2,00}) - (y_3 - y_2)]$, $[(dy_1/dt) - (dy_3/dt)]$, and $[(dy_2/dt) - (dy_3/dt)]$ must fall so that the axial motion mode will be stable. These conditions must also exist within a time range defined as t - 0.005 sec to t + 0.005 sec, if the ideal nominal starting time of the cycle is t.[3] These conditions can be written as

$$- 0.5 \text{ ft} < [(y_{2,00} - y_{1,00}) - (y_2 - y_1)] < + 0.5 \text{ ft}, \tag{53}$$

$$- 0.5 \text{ ft} < [(y_{3,00} - y_{2,00}) - (y_3 - y_2)] < + 0.5 \text{ ft}, \tag{54}$$

$$\left(\frac{dy_1}{dt} - \frac{dy_3}{dt}\right) \le V_0, \tag{55}$$

$$V_1 < \left(\frac{dy_2}{dt} - \frac{dy_3}{dt}\right) < V_2, \tag{56}$$

where V_0, V_1, and V_2 are given constants (see Ref. 4). Practically, for the configuration investigated, the values of V_o, V_1, and V_2 were V_0 = -58 ft/sec, V_1 = -40 ft/sec, V_2 = -25 ft/sec.

III. ANALOG-COMPUTER PROGRAM

Because of lack of time and funds, the complete engine simulation could not be attempted, so only the nine equations of motion, Eqs. (31) through (40), and their corresponding restoring force and moment equations, (10) through (30), could be programmed. The system operating equations (41) through (53) could not be included, and this, as will be seen in Section V, precluded the multi-cycle sequenced engine operation simulation. Nevertheless, the part of the program that was completed was used to simulate single cycles. Also, a portion of the existing program was rewired to simulate the operation of an experimental toroidal shock absorber that was dynamically tested a few years ago.[9] This was used as a check to ensure that the cross-coupling between the lateral and tilting motion modes had been correctly programmed for the torus-system spring.

The analytical equations given in Section 2 were rearranged to minimize the equipment required and also to maximize the accuracy of the simulation. For instance, the equations of the first spring were rewritten so that data already at hand[6] could be used directly, with the use of function generators. The numerical equations, corresponding to a 500-ton vehicle, 10-m-diam engine optimized as shown in Ref. 3, are given below.

3.1. TORUS-SYSTEM RESTORING FORCE AND MOMENT EQUATIONS

Using Eqs. (19) and (20), the lateral restoring force for each torus stack can be expressed as

$$F(x_2-x_1)_i = \frac{k_i\,(x_1 - x_2)\,D_i^3 - 3g(\alpha)\cdot(y_{2,00} - y_{1,00})\,M_i}{2(y_{2,00} - y_{1,00})\,g(\alpha)\,(y_2 - y_1) + D_i^2\,h(\beta)} ,$$

where

$$g(\alpha) = \frac{4(1 - \alpha)}{3\pi\ K_{nx}\ f(\alpha)} \text{ and } h(\beta) = \frac{\sigma_0}{E_0 \sin\beta_0 \sin\beta \cos\beta}$$

if

$$\alpha = \frac{(y_{2,00} - y_{1,00}) - (y_2 - y_1)}{(y_{2,00} - y_{1,00})} = \frac{\Delta y}{d} ,$$

and for the complete torus system,

$$F(x_2 - x_1) = \sum_{i=1}^{5} F(x_2 - x_1)_i .$$

Similarly, the restoring moment equations (28) and (29) can be combined and

$$M(\Theta_2 - \Theta_1)_i = \frac{k_i(\Theta_1 - \Theta_2)\ D_i^3 - \ell(\alpha)\ (y_2 - y_1)\ F(x_2 - x_1)_i}{2\ell(\alpha)} ,$$

where

$$\ell(\alpha) = \frac{4}{\pi\ K_{nx}\ f(\alpha)} ,$$

and for the complete torus system,

$$M(\Theta_2 - \Theta_1) = \sum_{i=1}^{5} M(\Theta_2 - \Theta_1)_i .$$

These equations were used in the analog computer program to eliminate the calculation of Θ^* and x^*.

The functions of α, $g(\alpha)$ and $\ell(\alpha)$, and also $h(\beta)$ were programmed on diode function generators (DFG). The curves representing these functions are given in Appendix C.

3.2. NUMERICAL EQUATIONS

All equations given in Section 2.1. and used in the analog computer program are given below in their numerical form for both the problem time scale and the program time scale. Time-scaling was used to slow down the system oscillations to minimize the errors caused by the equipment response and also to allow manual cycling of the system. The program time scale is 10/1 that of the problem (real time), in other words, a program single cycle (τ) lasts 10 sec instead of 1 sec (normal firing period) and therefore $\tau = 10t$.

For the values of the various coefficients given in Appendix D, the numerical differential equations are as follows:

First Mass (M_1) (Axial Motion)

$$\ddot{y}_1 = -0.1572\ (\dot{y}_1 - \dot{y}_2) - 581.4\alpha + 1.747 \times 10^4\ \alpha^4 \qquad \text{for } \alpha < 0,$$

$$\ddot{y}_1 = -0.1572\ (\dot{y}_1 - \dot{y}_2) - 422.7\alpha - 602.1\ \alpha^2 \qquad \text{for } \alpha \geq 0,$$

or for $\tau = 10t$,

$$\frac{d^2y_1}{d\tau^2} = -0.01572 \left(\frac{dy_1}{d\tau} - \frac{dy_2}{d\tau}\right) - 5.814\ \alpha + 174.7\ \alpha^4,$$

$$\frac{d^2y_1}{d\tau^2} = -0.01572 \left(\frac{dy_1}{d\tau} - \frac{dy_2}{d\tau}\right) - 4.227\ \alpha - 6.021\ \alpha^2,$$

respectively.

Second Mass (M_2) (Axial Motion)

$$\ddot{y}_2 = -7.663\,\ddot{y}_1 - 65.78\,\ddot{y}_3\ ;$$

also, for $\tau = 10t$,

$$\frac{d^2y_2}{d\tau^2} = -7.663\,\frac{d^2y_1}{d\tau^2} - 65.78\,\frac{d^2y_3}{d\tau^2}\ .$$

Third Mass (M_3) (Axial Motion)

$$\ddot{y}_3 = -5.495 \times 10^{-3}\,(\dot{y}_3 - \dot{y}_2) - 10.48\,(y_3 - y_2) + 576.2 \qquad \text{for } -S < \gamma < +S,$$

$$\ddot{y}_3 = -5.495 \times 10^{-3}\,(\dot{y}_3 - \dot{y}_2) - 0.4029\,(y_3 - y_2) + 32.23 \qquad \text{for } \gamma > +S,$$

$$\ddot{y}_3 = -5.495 \times 10^{-3}\,(\dot{y}_3 - \dot{y}_2) - 0.4029\,(y_3 - y_2) + 12.09 \qquad \text{for } \gamma < -S$$

if

$$\gamma = (y_{3,00} - y_{2,00}) - (y_3 - y_2),$$

or for $\tau = 10t$,

$$\frac{d^2y_3}{d\tau^2} = -5.495 \times 10^{-4}\left(\frac{dy_3}{d\tau} - \frac{dy_2}{d\tau}\right) - 0.1048\,(y_3 - y_2) + 5.762,$$

$$\frac{d^2y_3}{d\tau^2} = -5.495 \times 10^{-4}\left(\frac{dy_3}{d\tau} - \frac{dy_2}{d\tau}\right) - 4.029 \times 10^{-3}\,(y_3 - y_2) + 0.3223,$$

$$\frac{d^2y_3}{d\tau^2} = -5.495 \times 10^{-4}\left(\frac{dy_3}{d\tau} - \frac{dy_2}{d\tau}\right) - 4.029 \times 10^{-3}\,(y_3 - y_2) + 0.1209,$$

respectively.

First Mass (M_1) (Lateral Motion)

$$\ddot{x}_1 = -0.7863\ (\dot{x}_1 - \dot{x}_2) - 3.145 \times 10^{-2} \sum_{i=1}^{5} F(x_2-x_1)_i$$

or for $\tau = 10t$,

$$\frac{d^2x_1}{d\tau^2} = -0.07863 \left(\frac{dx_1}{d\tau} - \frac{dx_2}{d\tau}\right) -3.145 \times 10^{-4} \sum_{i=1}^{5} F(x_2 - x_1)_i$$

where

$$F(x_2-x_1)_1 = j_1(\alpha)\ [2.163 \times 10^5\ (x_1 - x_2) - 24g(\alpha)\ M(\Theta_2 - \Theta_1)_1]$$

$$F(x_2-x_1)_2 = j_2(\alpha)\ [1.505 \times 10^6\ (x_1 - x_2) - 24g(\alpha)\ M(\Theta_2 - \Theta_1)_2]$$

$$F(x_2-x_1)_3 = j_3(\alpha)\ [1.782 \times 10^6\ (x_1 - x_2) - 24g(\alpha)\ M(\Theta_2 - \Theta_1)_3]$$

$$F(x_2-x_1)_4 = j_4(\alpha)\ [4.029 \times 10^6\ (x_1 - x_2) - 24g(\alpha)\ M(\Theta_2 - \Theta_1)_4]$$

$$F(x_2-x_1)_5 = j_5(\alpha)\ [1.061 \times 10^7\ (x_1 - x_2) - 24g(\alpha)\ M(\Theta_2 - \Theta_1)_5]$$

The $j_i(\alpha)$ shown in Fig. 28 of Appendix C are defined as

$$j_i(\alpha) = \frac{1}{2(y_{2,00} - y_{1,00})(y_2 - y_1)\ g(\alpha) + D_i^2\ h(\beta)}\ .$$

Second Mass (M_2) (Lateral Motion)

$$\ddot{x}_2 = -7.663\ \ddot{x}_1 - 65.78\ \ddot{x}_3\ ;$$

for $\tau = 10t$,

$$\frac{d^2x_2}{d\tau^2} = -7.663\,\frac{d^2x_1}{d\tau^2} - 65.78\,\frac{d^2x_3}{d\tau^2}\,.$$

<u>Third Mass (M_3) (Lateral Motion)</u>

$$\ddot{x}_3 = -6 \times 10^{-2}\,(\dot{x}_3 - \dot{x}_2) + 1.099 \times 10^{5}\,(20 - \gamma)^{-3}\left(x_3 - x_2 \pm t_1\,\frac{t}{t_1}\right)$$

$$\text{if } -t > x_2 - x_3 > +t,$$

$$\ddot{x}_3 = -6 \times 10^{-3}\,(\dot{x}_3 - \dot{x}_2) \quad \text{if } -t < x_2 - x_3 < +t,$$

or for $\tau = 10t$,

$$\frac{d^2x_3}{d\tau^2} = -6 \times 10^{-3}\,(\dot{x}_3 - \dot{x}_2) + 1.099 \times 10^{3}\,(20 - \gamma)^{-3}\left(x_3 - x_2 \pm t_1\,\frac{t}{t_1}\right)$$

$$\frac{d^2x_3}{d\tau^2} = -6 \times 10^{-3}\,(\dot{x}_3 - \dot{x}_2)\,,$$

respectively.

<u>First Mass (M_1) (Tilting Motion)</u>

$$\ddot{\theta}_1 = -10^{-3}\,(\dot{\theta}_1 - \dot{\theta}_2) - 7.143 \times 10^{-4}\sum_{i=1}^{5} M(\theta_2 - \theta_1)_i$$

or for $\tau = 10t$,

$$\frac{d^2\theta_1}{d\tau^2} = -10^{-5}\left(\frac{d\theta_1}{d\tau} - \frac{d\theta_2}{d\tau}\right) - 7.143 \times 10^{-6} \sum_{i=1}^{5} M(\theta_2 - \theta_1)_i$$

where

$$M(\theta_2 - \theta_1)_1 = 2.163 \times 10^5 \left[\frac{1}{2\ \ell(\alpha)}\right] (\theta_1 - \theta_2) - \tfrac{1}{2}(y_2 - y_1)\ F(x_2 - x_1)_1 \ ,$$

$$M(\theta_2 - \theta_1)_2 = 1.505 \times 10^6 \left[\frac{1}{2\ \ell(\alpha)}\right] (\theta_1 - \theta_2) - \tfrac{1}{2}(y_2 - y_1)\ F(x_2 - x_1)_2$$

$$M(\theta_2 - \theta_1)_3 = 1.782 \times 10^6 \left[\frac{1}{2\ \ell(\alpha)}\right] (\theta_1 - \theta_2) - \tfrac{1}{2}(y_2 - y_1)\ F(x_2 - x_1)_3$$

$$M(\theta_2 - \theta_1)_4 = 4.029 \times 10^6 \left[\frac{1}{2\ \ell(\alpha)}\right] (\theta_1 - \theta_2) - \tfrac{1}{2}(y_2 - y_1)\ F(x_2 - x_1)_4$$

$$M(\theta_2 - \theta_1)_5 = 1.061 \times 10^7 \left[\frac{1}{2\ \ell(\alpha)}\right] (\theta_1 - \theta_2) - \tfrac{1}{2}(y_2 - y_1)\ F(x_2 - x_1)_5$$

<u>Second Mass (M_2) (Tilting Motion)</u>

$$\ddot{\theta}_2 = -10\ \ddot{\theta}_1 - 800\ \ddot{\theta}_3 \ ,$$

also, for $\tau = 10t$,

$$\frac{d^2\theta_2}{d\tau^2} = -10\ \frac{d^2\theta_1}{d\tau^2} - 800\ \frac{d^2\theta_3}{d\tau^2} \ .$$

<u>Third Mass (M_3)(Tilting Motion)</u>

$$\ddot{\theta}_3 = -8.929 \times 10^{-2}\ (\dot{\theta}_3 - \dot{\theta}_2) + 22.32\ (20 - \gamma)^{-1}\ [(\theta_3 - \theta_2) + 0.1\ (x_3 - x_2)] \ ,$$

or for $\tau = 10t$,

$$\frac{d^2\theta_3}{d\tau^2} = -8.929 \times 10^{-3} \left(\frac{d\theta_3}{d\tau} - \frac{d\theta_2}{d\tau}\right) + 0.2232\ (20 - \gamma)^{-1} [(\theta_3 - \theta_2) + 0.1\ (x_3 - x_2)].$$

3.3. ANALOG COMPUTER PROGRAM

The above equations were programmed for operation at the Convair-Astronautics analog computer facility. A bank of three analog computers was used (two EAI - 31R and one EAI -31Q).

The wiring diagrams of the program are presented in Figs. 4 through 6. Each diagram corresponds to a motion mode (y, x, and θ); the connections between each one is quite obvious: signals from one diagram are sent to another through DFG (diode function generators) or MULT. (multipliers).

Each coefficient potentiometer is identified by a number and the corresponding coefficient potentiometer settings are given in Table 1.

3.4. EXPERIMENTAL-TORUS-SYSTEM SIMULATION PROGRAM

This system is described in detail in Ref. 9, where its characteristics are given. The calculations of the system's constants and coefficients corresponding to these characteristics are given in Appendix E. This system can be simulated by the following set of numerical equations, using the pertinent equations given in Section 2.1.

$$\ddot{y}_1 = -18\dot{y}_1 - 4 \times 10^3 [12.8y_1 - 4840y_1^4] \qquad \text{for } \alpha < 0 \ ,$$

$$\ddot{y}_1 = -18\dot{y}_1 - 4 \times 10^3 [9.32y_1 + 30.9y_1^4] \qquad \text{for } \alpha \geq 0 \ ,$$

or for $\tau = 10^2 t$,

$$\frac{d^2y_1}{d\tau^2} = -0.18 \frac{dy_1}{d\tau} - 5.117y_1 + 1.932 \times 10^3 y_1^4 \qquad \text{for } \alpha < 0 \ ,$$

$$\frac{d^2y_1}{d\tau^2} = -0.18 \frac{dy_1}{d\tau} - 3.722y_1 - 12.34y_1^2 \qquad \text{for } \alpha \geq 0;$$

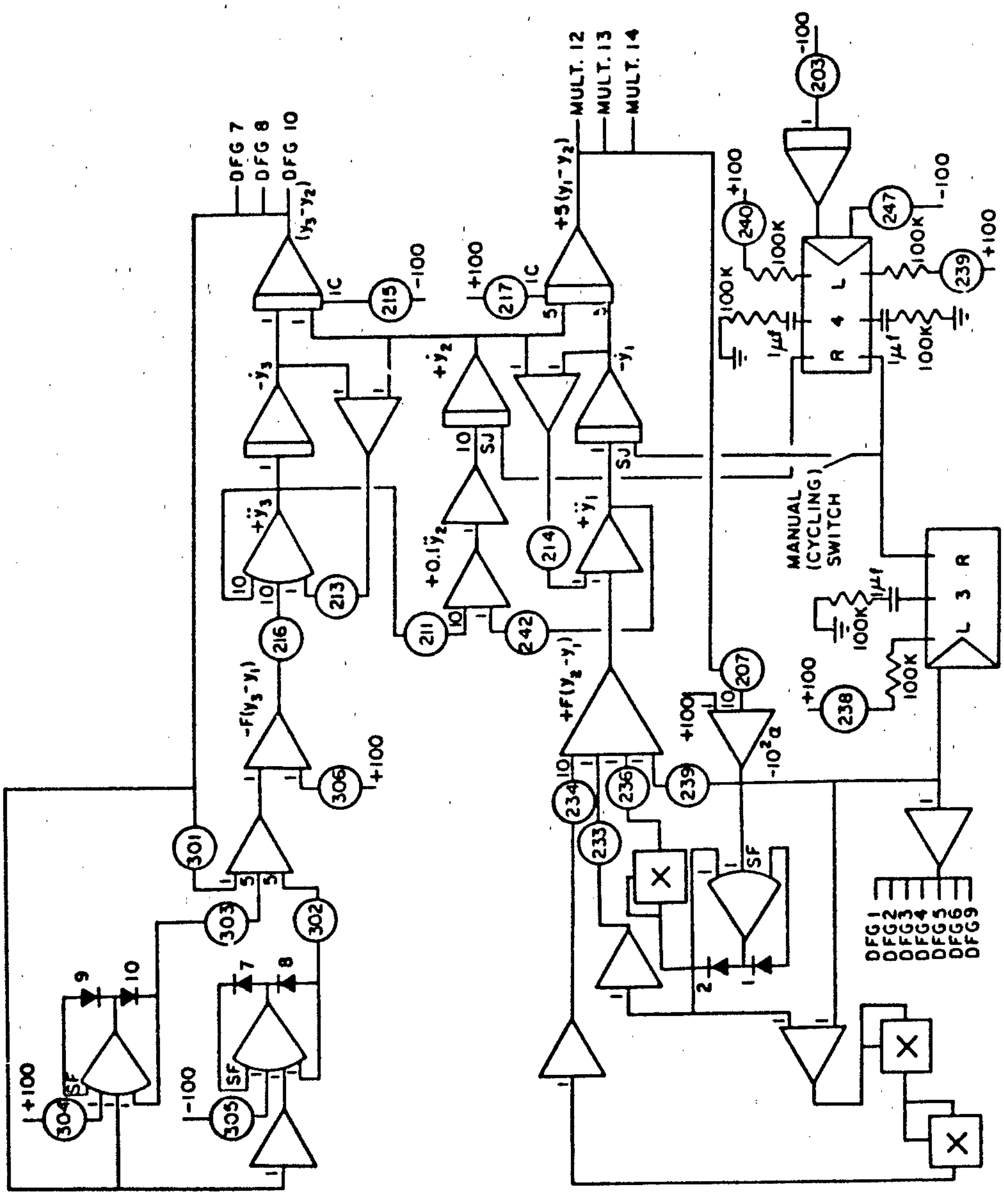

Fig. 4--Analog computer wiring diagram for axial motion mode

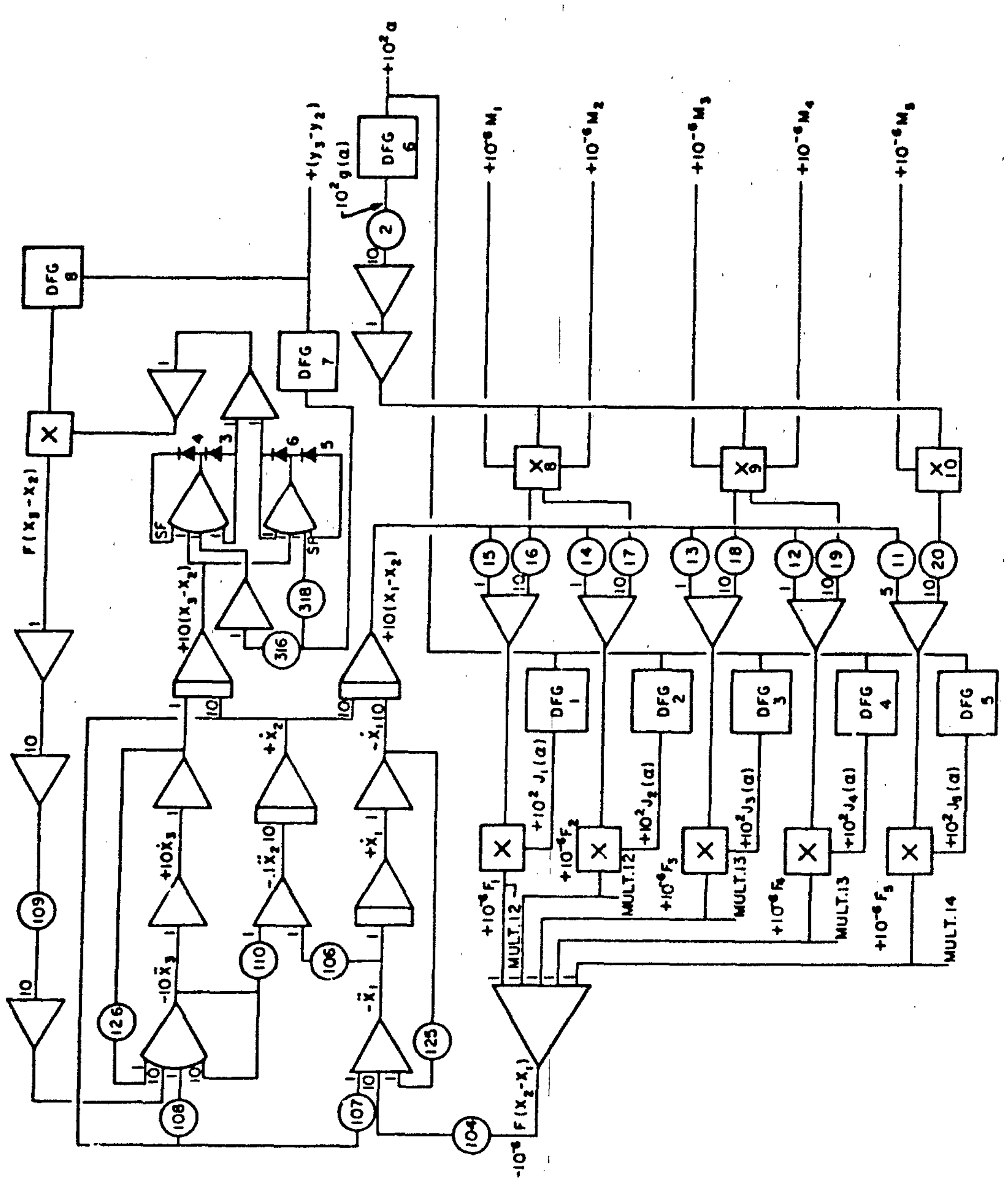

Fig. 5--Analog computer wiring diagram for lateral motion mode

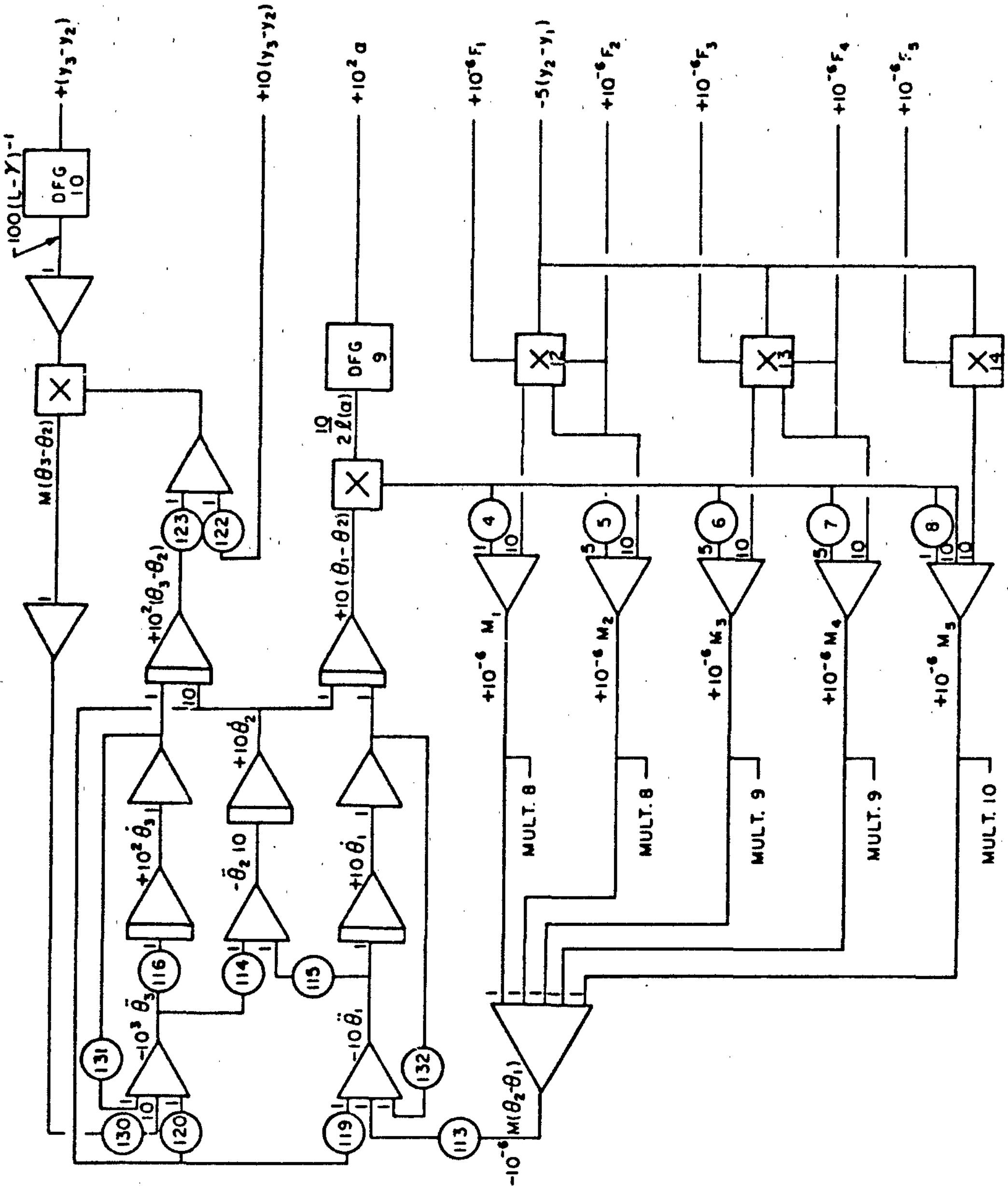

Fig. 6--Analog computer wiring diagram for tilting motion mode

Table 1

COEFFICIENT POTENTIOMETER SETTINGS

No.	Equation Coefficient	Setting	No.	Equation Coefficient	Setting
2	$0.1(3)$	0.3000	109	$10^{-4}(1/M_3)(t/\tau)^2$	0.1099
4	$10^{-6}\ k_1'D_1^3$	0.2163	110	$10^{-2}(M_3/M_2)$	0.6578
5	$2 \times 10^{-7}\ k_1'D_2^3$	0.3010	113	$10^5(1/I_1)(t/\tau)^2$	0.7143
6	$2 \times 10^{-7}\ k_1''D_3^3$	0.3564	114	$10^{-3}(I_3/I_2)$	0.8000
7	$2 \times 10^{-7}\ k_1''D_4^3$	0.8058	115	$0.1(I_1/I_2)$	1.0000
8	$10^{-6}\ k_1''D_5^3-10$	0.6100	116	0.1	0.1000
11	$2 \times 10^{-8}\ k_1''D_5^3$	0.2122	119	$(q_1/I_1)(t/\tau)$	0.1000
12	$10^{-7}\ k_1''D_4^3$	0.4029	120	$10^2(q_2/I_3)(t/\tau)$	0.8929
13	$10^{-7}\ k_1''D_3^3$	0.1782	122	$10^{-8}\ K_2(2/L)$	0.2500
14	$10^{-7}\ k_1'D_2^3$	0.1505	123	$10^{-8}\ K_2(2/L)$	0.2500
15	$10^{-7}\ k_1'D_1^3$	0.02163	125	$(r_1/M_1)(t/\tau)$	0.07863
16	$0.1(y_{2,00} - y_{1,00})$	0.8000	126	$10(r_2/M_3)(t/\tau)$	0.0600
17	$0.1(y_{2,00} - y_{1,00})$	0.8000	130	$10^9(1/I_3)(t/\tau)^2$	0.8929
18	$0.1(y_{2,00} - y_{1,00})$	0.8000	131	$10(q_2/I_3)(t/\tau)$	0.08929
19	$0.1(y_{2,00} - y_{1,00})$	0.8000	132	$(q_1/I_1)(t/\tau)$	0.1000
20	$0.1(y_{2,00} - y_{1,00})$	0.8000	203	Time generator	0.0125
104	$10^5(1/M_1)(t/\tau)^2$	0.3145	207	$2/(y_{2,00} - y_{1,00})$	0.01209
106	$0.1(M_1/M_2)$	0.7663	211	$0.01(M_3/M_2)$	0.6578
107	$(r_1/M_1)(t/\tau)$	0.07863	213	$(10p_2/M_3)(t/\tau)$	0.005495
108	$10^2(r_2/M_3)(t/\tau)$	0.6000	214	$(p_1/M_1)(t/\tau)$	0.01572

Table 1--continued

No.	Equation Coefficient	Setting	No.	Equation Coefficient	Setting
215	$0.01(y_{3,00} - y_{2,00})$	0.5500	242	$0.1(M_1/M_2)$	0.7663
216	$10^{-2}/M_3(t/\tau)^2$	0.3663	247	Impulse delay	0.0500
217	$0.05(y_{2,00} - y_{1,00})$	0.4000	301	10^{-5} C	0.1100
229	$(0.04A/M_1)(t/\tau)^2$	0.04227	302	2×10^{-6} B	0.5500
233	$(0.015A/M_1)(t/\tau)^2$	0.01587	303	2×10^{-6} B	0.5500
234	$(0.165A/M_1)(t/\tau)^2$	0.1747	304	$0.01(y_{3,00} - y_{2,00} - S)$	0.5400
236	$(0.057A/M_1)(t/\tau)^2$	0.06021	305	$0.01(y_{3,00} - y_{2,00} + S)$	0.5600
238	$10^{-3}\ \dot{y}_1\ (\alpha \approx 0)$	0.1260	306	$10^{-7}\left[B + C(y_{3,00} - y_{2,00})\right]$	0.0880
239	$10^{-3}\ \dot{y}_{1,00}$	0.0650	316	t_1	0.00200
240	$10^{-3}\ \dot{y}_{2,00}$	0.0385	318	t_1	0.00200

$$\ddot{x}_1 = - 30\ \dot{x}_1 - J(\alpha)\ [9200x_1 - 5.16g(\alpha)\ M(\theta)]$$

or for $\tau = 10^2t$,

$$\frac{d^2x_1}{d\tau^2} = - 0.3\ \frac{dx_1}{d\tau} - J(\alpha)\ [0.92x_1 - 5.16 \times 10^{-4}\ g(\alpha)\ M(\theta)];$$

$$\ddot{\theta}_1 = - 62.4\ \dot{\theta}_1 - 47.17\left[\frac{2.3 \times 10^3\ \theta_1}{2\ell(\alpha)} - 0.5(y_2 - y_1)\ F(x)\right]$$

or for $\tau = 10^2t$,

$$\frac{d^2\theta_1}{d\tau^2} = - 0.624\ \frac{d\theta_1}{d\tau} - \frac{10.85}{2\ell(\alpha)}\ \theta_1 + 2.359 \times 10^{-5}(y_2 - y_1)\ F(x),$$

where $M(\theta)$ and $F(x)$ are the restoring moment and restoring force, respectively; $j(\alpha)$ was recomputed for $D_1 = 1$ ft.

The wiring diagram for this set of equations is shown in Fig. 7 and the coefficient potentiometer settings are presented in Table 2.

IV. RESULTS

Each degree of freedom for the three masses was investigated separately to determine its own characteristics and to ensure that the model operated properly. The lateral stability study was not completed since the equations representing the sequenced random off-nominal and off-centered impulses could not be programmed. Therefore, the present investigation was limited to single-impulse operation of the complete system for a fully loaded vehicle only. Although the study is incomplete, it is possible to predict whether the system operation might be stable and what conditions would have to be fulfilled to ensure stability should the configuration under study prove to be unstable. Therefore, the single-impulse operation was thoroughly investigated. The results obtained so far are reported below in chronological order.

4.1 ON-AXIS MOTION STUDY

This motion, which corresponds to the axial displacement of the three masses, is mathematically described by Eqs. (31) through (33). This mode has been extensively investigated in the past using digital computer techniques[3][4] and operation stability criteria were defined. The purpose of study described here was to ensure that the results obtained with the analog computer program were identical to those reported in Refs. 3 and 4 for single-impulse operation and also to confirm that

1. Repeated nominal impulses delivered at the correct time would lead to a stable operation for the longitudinal mode.
2. Single impulses corresponding to the upper and lower tolerances on the momentum imparted to the vehicle would not create a misfire condition[3] and therefore were compatible with a continuous operation.

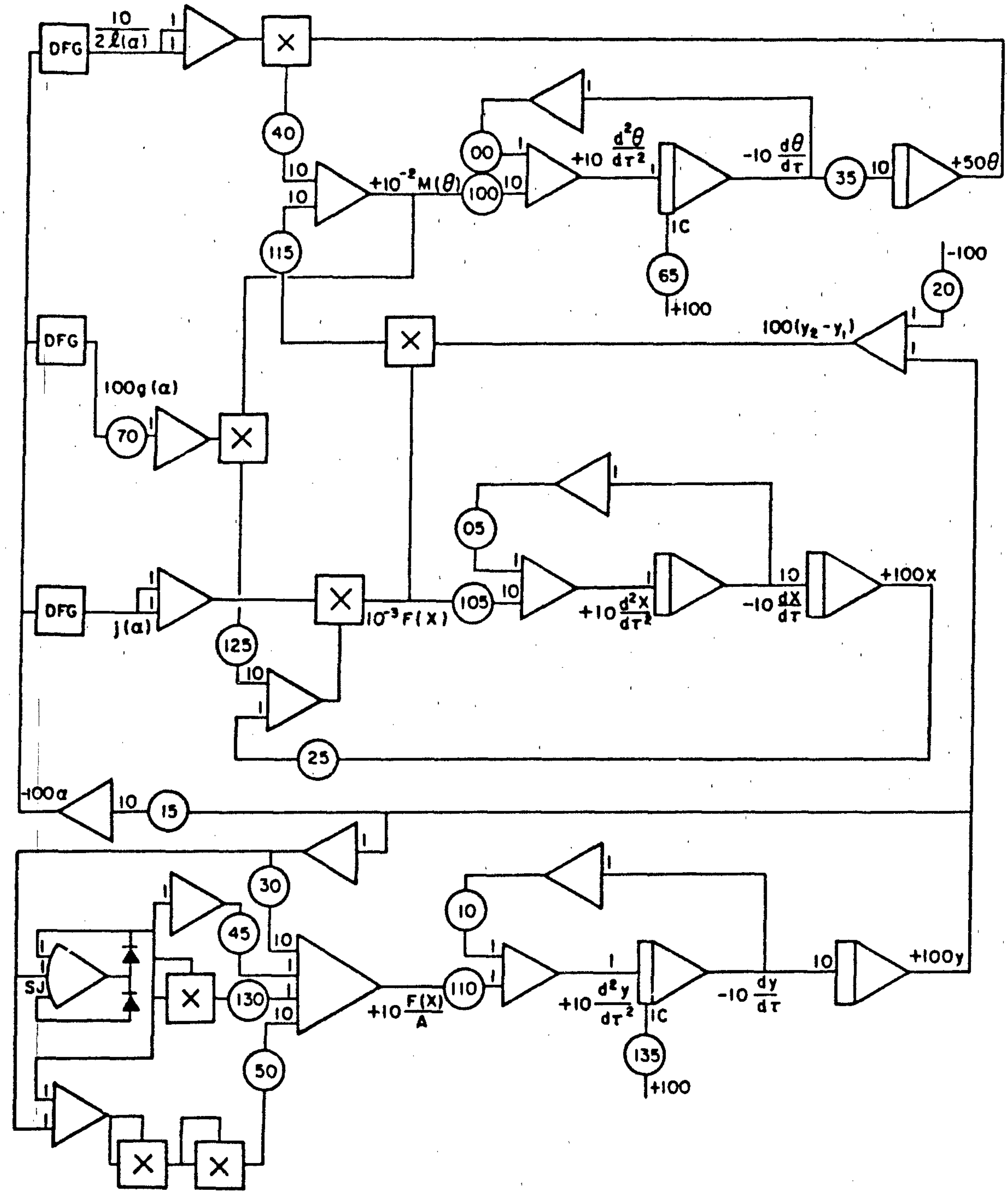

Fig. 7--Analog computer wiring diagram for experimental torus-system simulation

Table 2

COEFFICIENT POTENTIOMETER SETTINGS

No.	Equation Coefficient	Setting
00	$(q_1/I_1)(t/\tau)$	0.6250
05	$(r_1/m_1)(t/\tau)$	0.3000
10	$(p_1/m_1)(t/\tau)$	0.1800
15	$10[1/(y_{2,00} - y_{1,00})](y_1/\gamma)$	0.2326
20	y_2	0.4300
25	$0.5 \times 10^{-3} K_1 D^3$	0.2750
30	$5.5[1/(y_{2,00} - y_{1,00})]10^{-2}$	0.1279
35	0.5	0.5000
40	$10^{-4} K_1 D^3$	0.1000
45	$1.5[1/(y_{2,00} - y_{1,00})]10^{-1}$	0.3489
50	$165[1/(y_{2,00} - y_{1,00})]^4 \, 10^{-4}$	0.4830
100	$10^2(1/I_1)(t/\tau)^2$	0.4717
105	$10^3(1/m_1)(t/\tau)^2$	0.4000
110	$A(1/m_1)(t/\tau)^2$	0.4200
115	0.5	0.5000
125	$0.5[3(y_{2,00} - y_{1,00})]$	0.6450
130	$5.7[1/(y_{2,00} - y_{1,00})]^2/10^{-3}$	0.03084
135	$10\dot{y}_{1,00}(t/\tau)10^{-2}$	0.0400
65	$10 \, \dot{\theta}_{1,00}(t/\tau)10^{-2}$	0.0800
70	g_1/g	0.9500

3. Repeated impulses, systematically chosen at the upper or lower tolerance limits, would not lead to rapidly diverging amplitudes.

The results presented in Fig. 8 substantiate the three points above. After the fifth impulse, one sees that the system dynamic operation does not deteriorate appreciably for both maximum and minimum off-nominal impulses when compared to the nominal impulse. A considerably larger amount of information about the velocities and the spring reactions was also obtained which confirmed the conditions itemized above. The curves of Fig. 9 demonstrate the repeatability of the intermediate-platform velocity profile for the nominal impulse.

The on-axis dynamic characteristics of the system were deemed quite satisfactory at this point.

4.2. LATERAL MOTION STUDY

Equations (34) through (36) correspond to this motion mode. The system was submitted to a side impulse simulated by a momentum delivered to mass M_1. The lateral oscillating motion of M_1 was studied for when no longitudinal impulse is delivered on the pusher plate (the pusher remains in the neutral position) and when a nominal axial impulse is delivered on the pusher. From a comparison of these two conditions, the influence of the longitudinal motion on the lateral oscillation can be determined. The results are presented in Fig. 10 for the first and in Fig. 11 for the second. The influence of the on-axis motion is extremely pronounced because of the large stiffening effect of the second spring during the compression cycle and to its decreased stiffness during the "misfire" cycle. Although no angular impulse was given to M_1, the cross-coupling existing between the x_1 displacements and the Θ_1, as demonstrated in Ref. 6, excites oscillations of M_1 in the Θ mode. The curves of Figs. 12 and 13 indicate that this cross-coupling effect is rather large.

4.3. TILTING MOTION STUDY

The rotation of masses M_1 and M_2 was then investigated; these correspond to Eqs. (37) through (39). Again both cases, without and with longitudinal impulse, were investigated. As explained in Ref. 6, there is

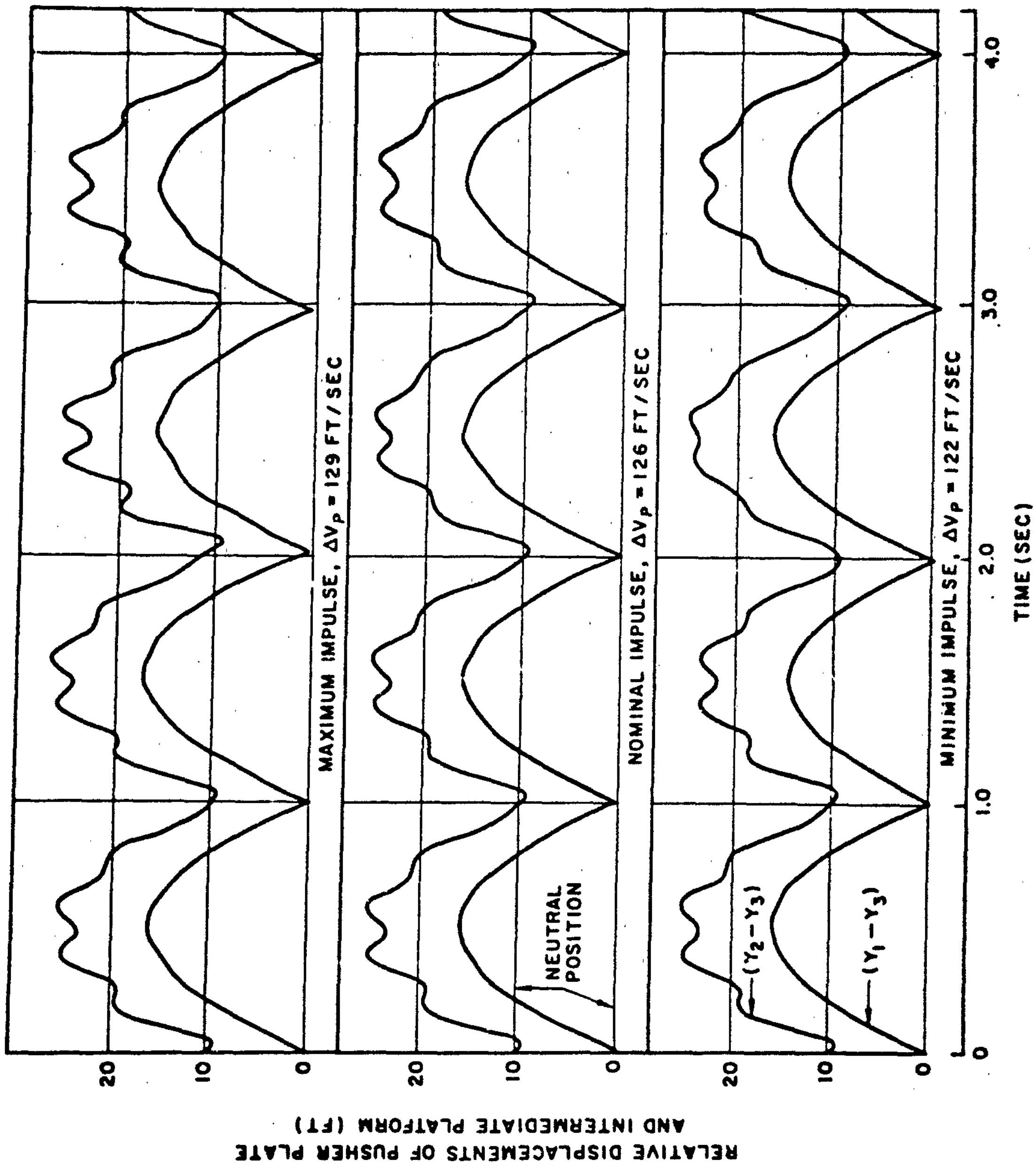

Fig. 8--Typical longitudinal motion mode

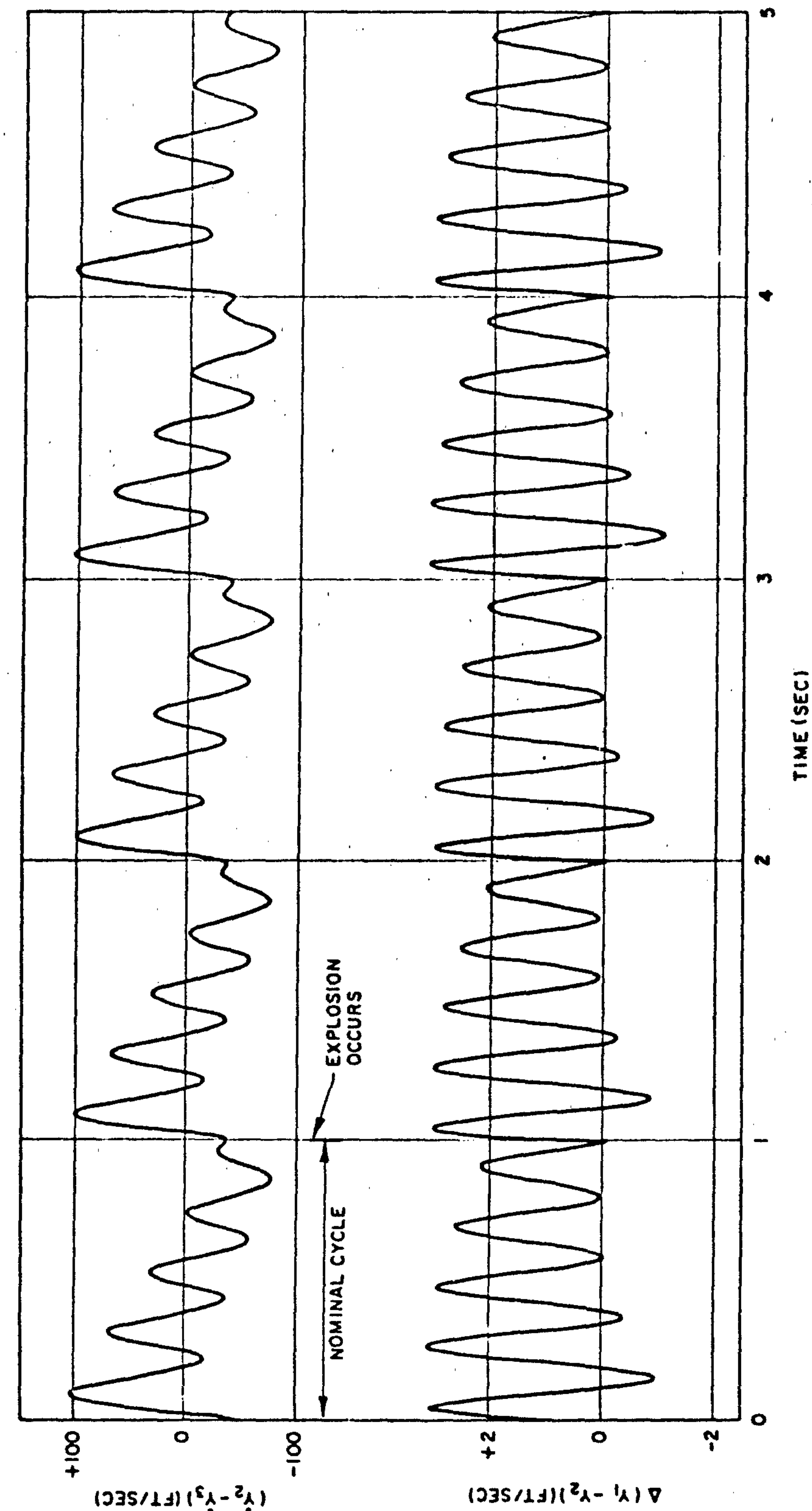

Fig. 9--Typical (M_2 - M_3) velocity and (M_1 - M_2) displacement vs time for nominal cycle

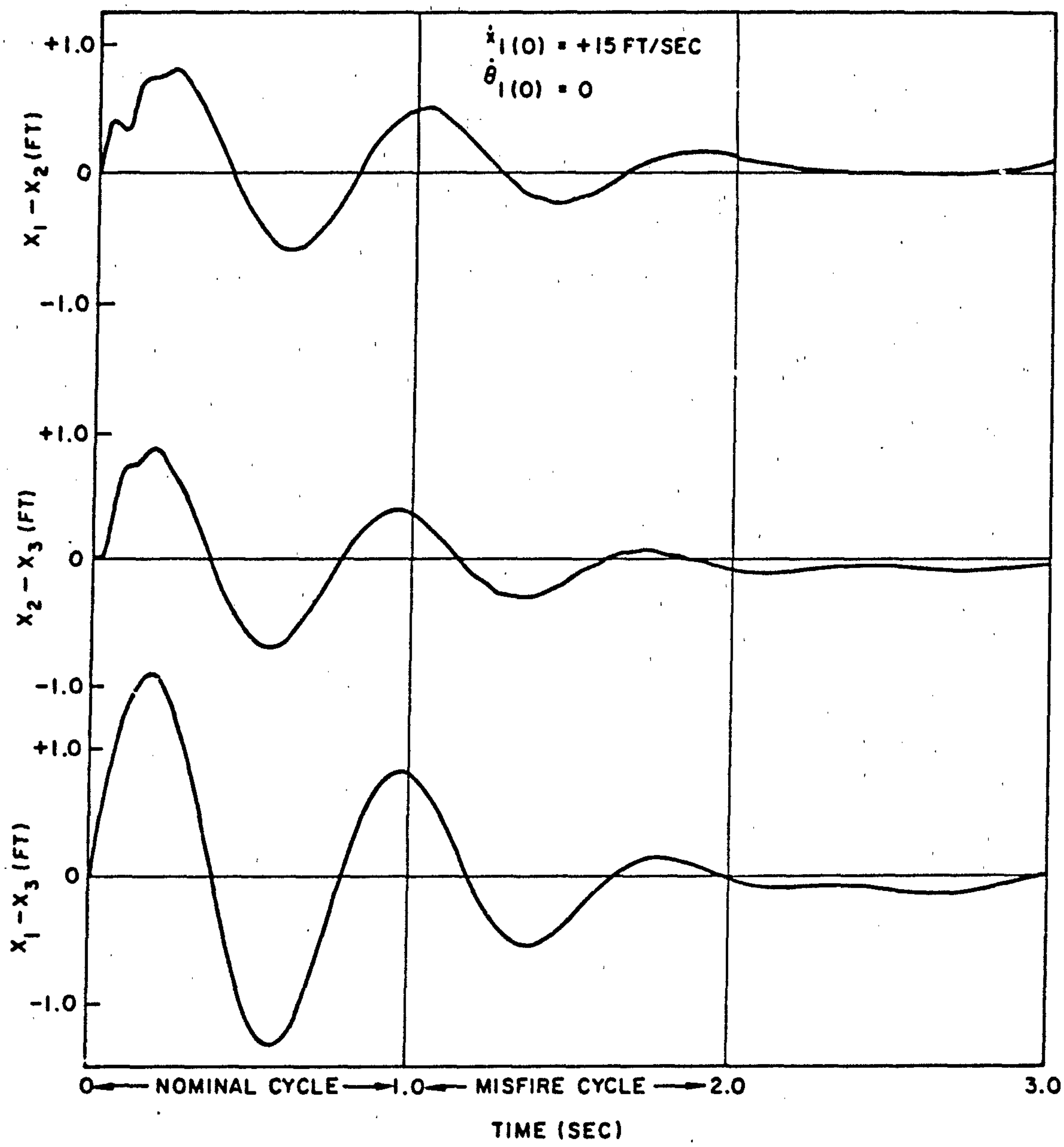

Fig. 10--Lateral motion--no axial motion (lateral impulse only)

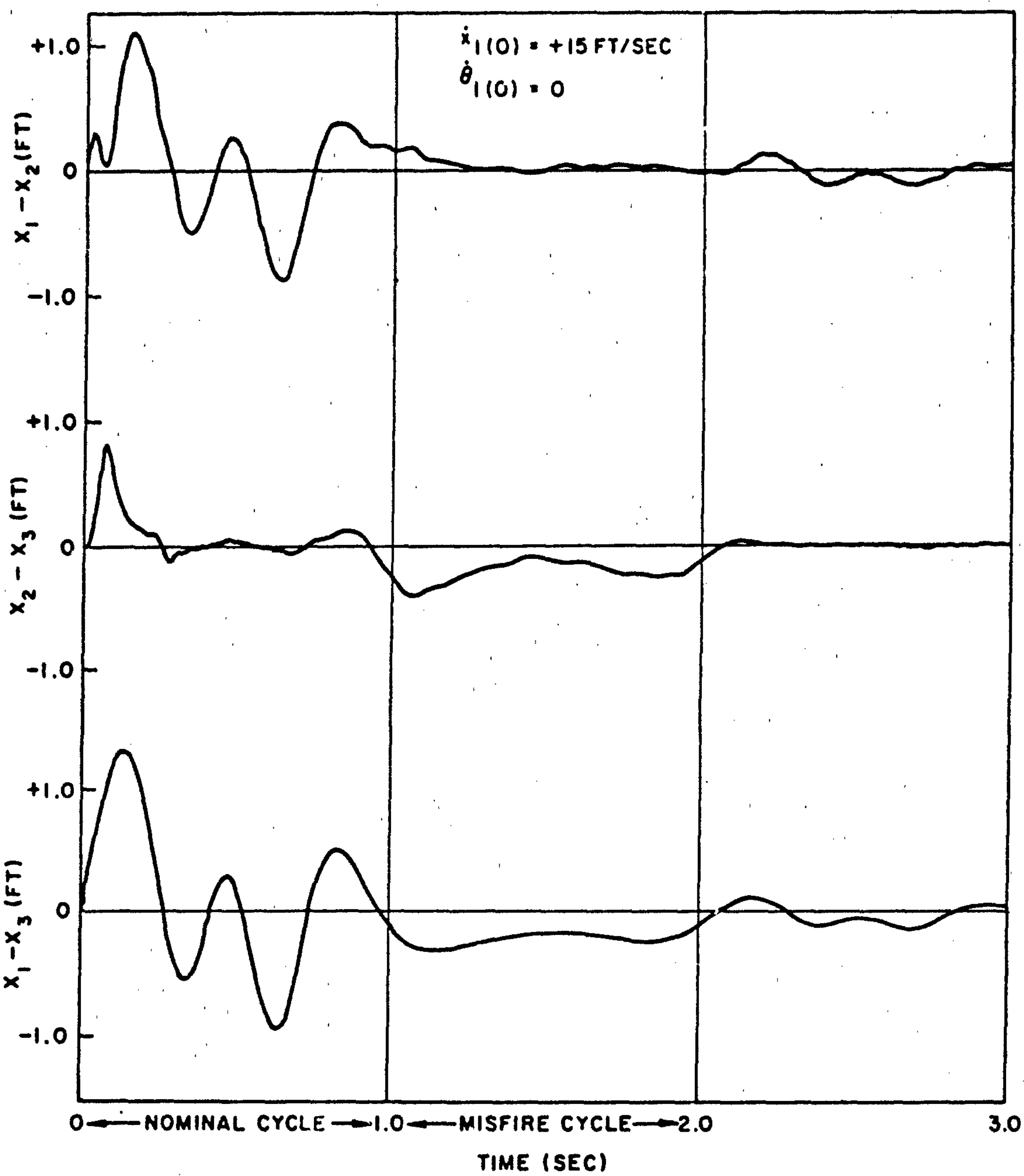

Fig. 11--Lateral motion--with axial motion (lateral impulse only)

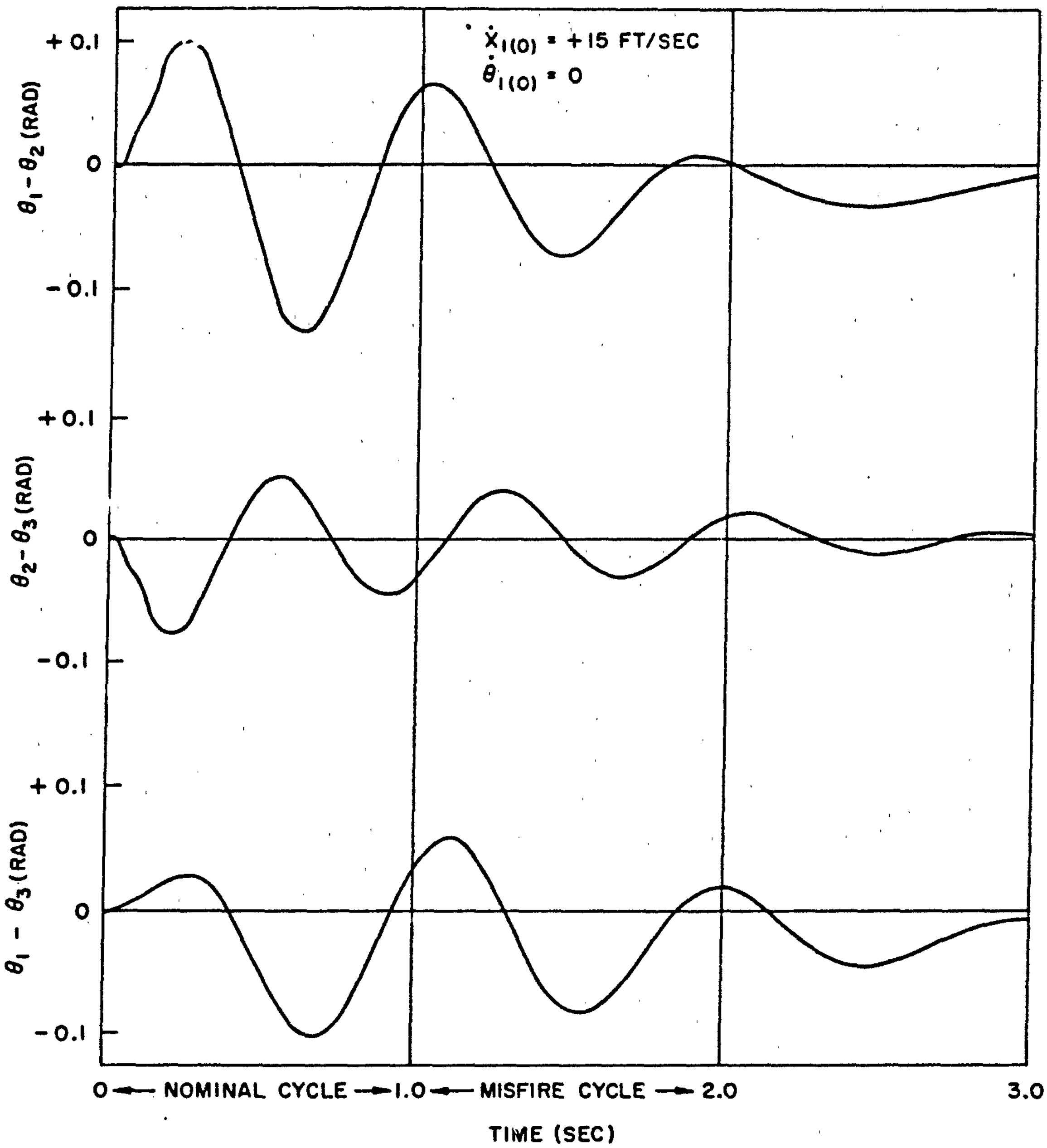

Fig. 12--Lateral motion--no axial motion (influence of cross-coupling)

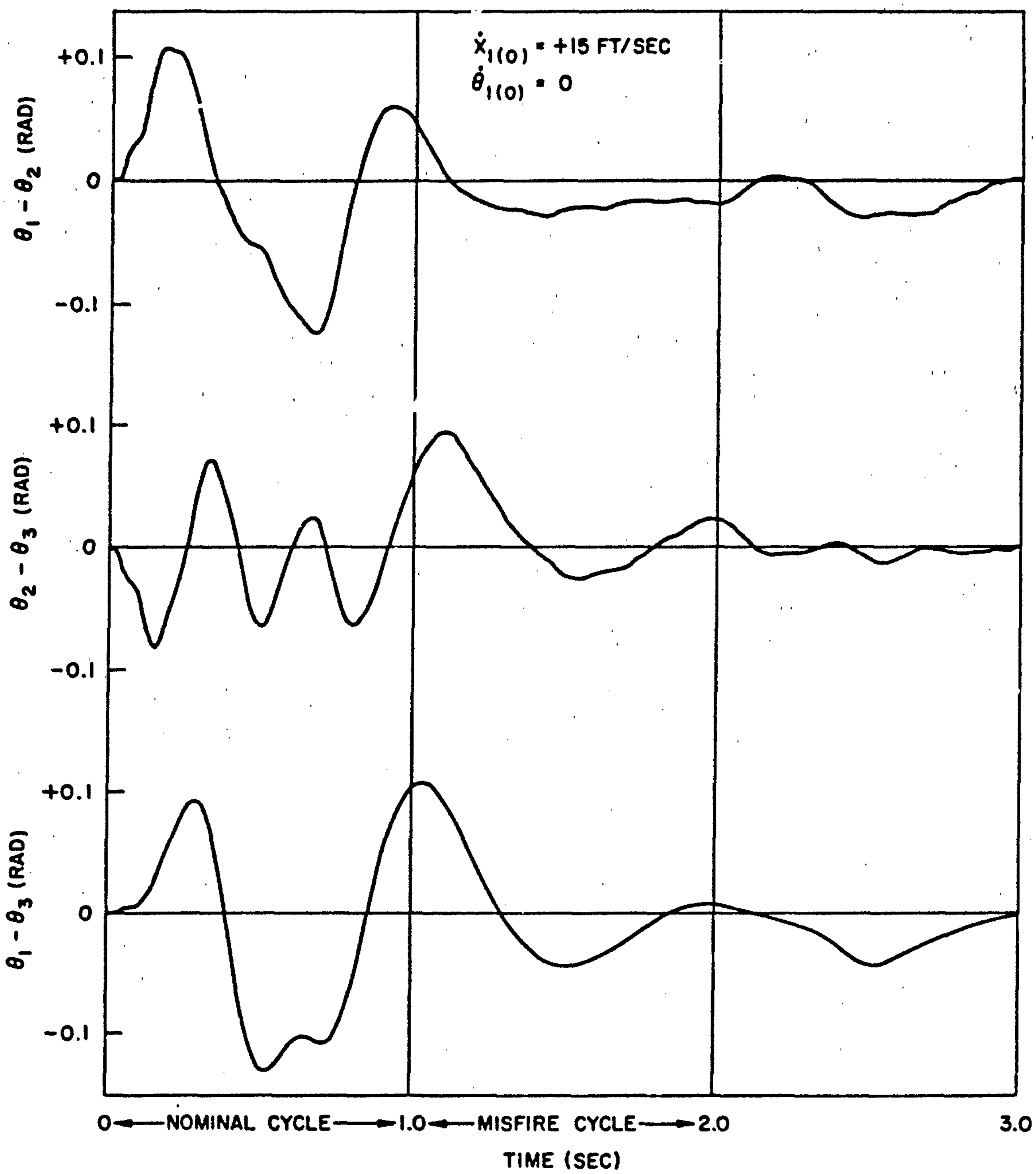

Fig. 13--Lateral motion--with axial motion (influence of cross-coupling)

also a cross-coupling present in the system between lateral and tilting motions of mass M_1.

An initial angular momentum was delivered to M_1 and the system was let free to oscillate. The results are presented in Figs. 14 through 17. The cross-coupling influence is also large in this case.

4.4. COMBINED MOTION STUDY

Finally, an initial impulse was delivered to mass M_1 for the three modes of oscillation for two typical cases: with mass M_1 in the neutral position and with mass M_1 tilted 0.1 rad so that this tilting could justify the lateral impulse given to M_1, as explained in Section 5.

The results are given in Figs. 18 through 25. The initial conditions given on each figure are self-explanatory.

4.5. EXPERIMENTAL-TORUS-SYSTEM SPRING SIMULATION

For this simulation, spring stiffnesses, damping coefficients, and velocity initial conditions were varied to try to obtain a good similarity with the curves of Figs. 33 through 40 of Ref. 9. But in all cases, only two initial conditions, $\dot{\theta}_{1(0)}$ and $\dot{y}_{1(0)}$, were set different from zero so that the experiments reported in Ref. 9 could be accurately simulated. The lateral motion induced by the tilting motion of the plate was therefore caused only by the cross-coupling effects, as previously shown in Figs. 12, 13, 16 and 17.

The best matching of the analog computer results with those of Ref. 9 was obtained for values of equation coefficients different from those calculated in Appendix E. This was to be expected since the toroidal shock-absorber model tested was not built as ideally as it could be now.(3) Also, the testing was conducted with atmospheric pressure surrounding the system, which affected the system dynamic behavior. The best results obtained with the analog computer are presented in Fig. 26 where the axial lateral and angular displacements of the plate are compared with the most pertinent curves given in Ref. 9.

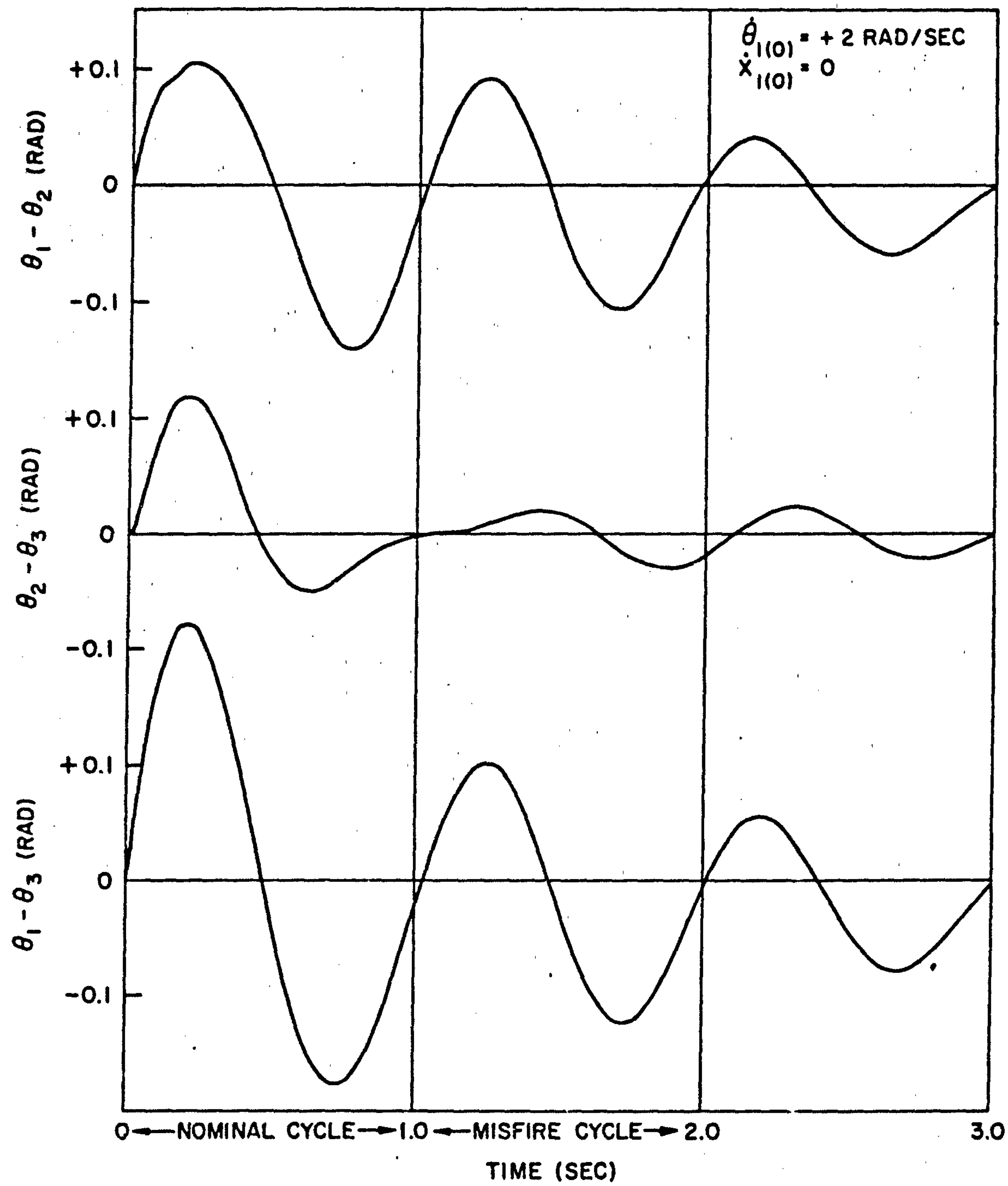

Fig. 14--Tilting motion--no axial motion (angular impulse only)

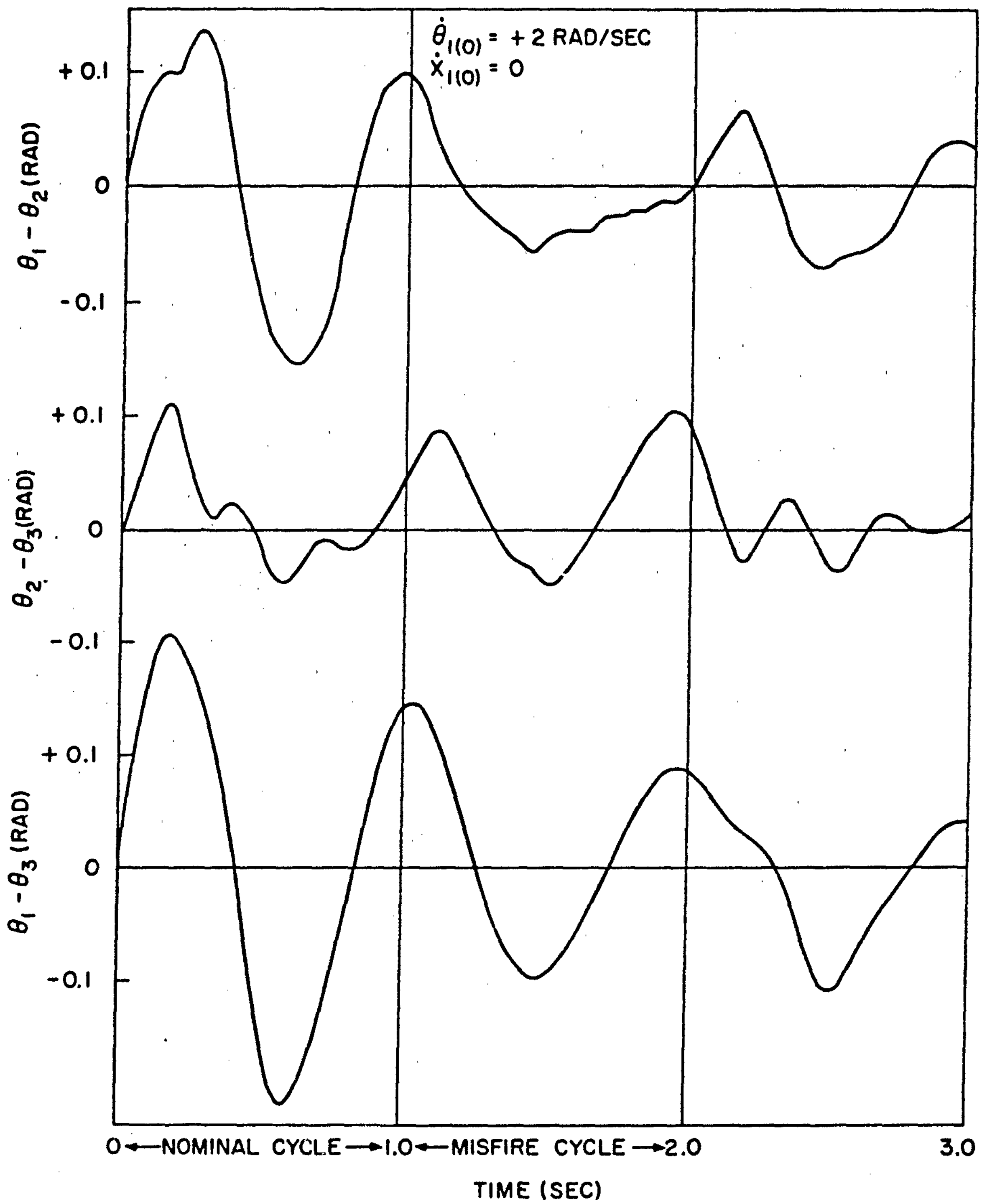

Fig. 15--Tilting motion--with axial motion (angular impulse only)

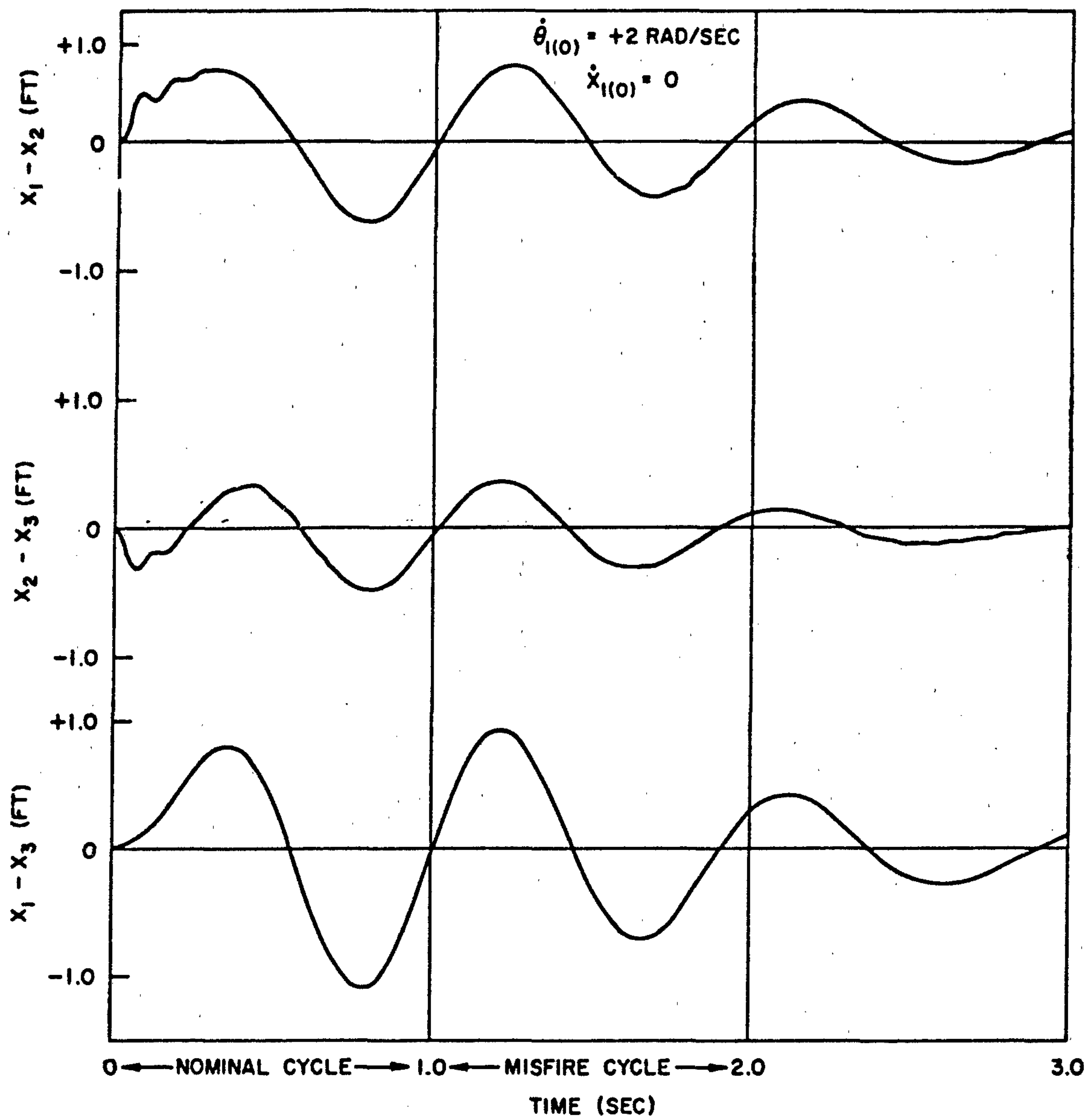

Fig. 16--Tilting motion--no axial motion (influence of cross-coupling)

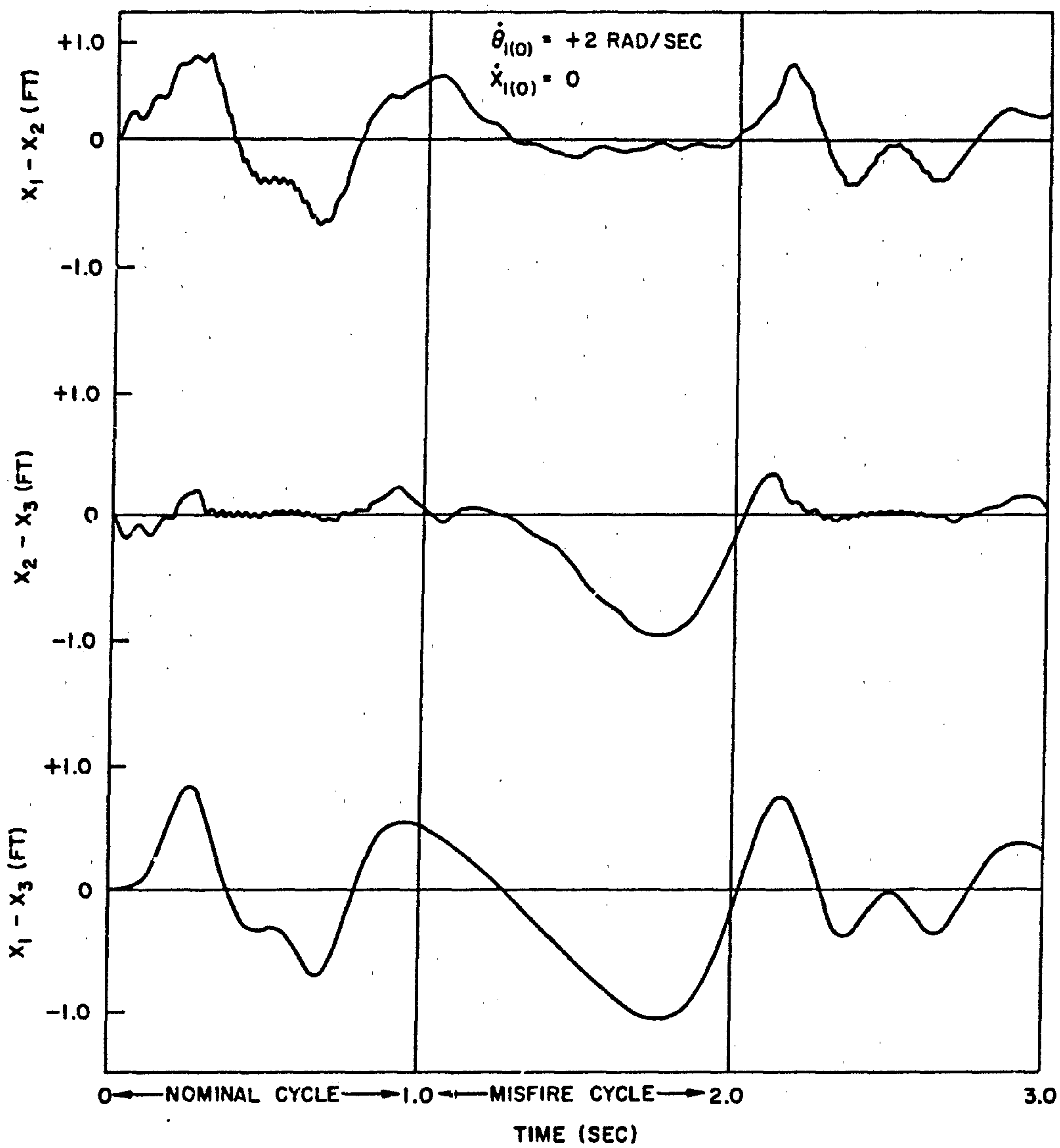

Fig. 17--Tilting motion--with axial motion (influence of cross-coupling)

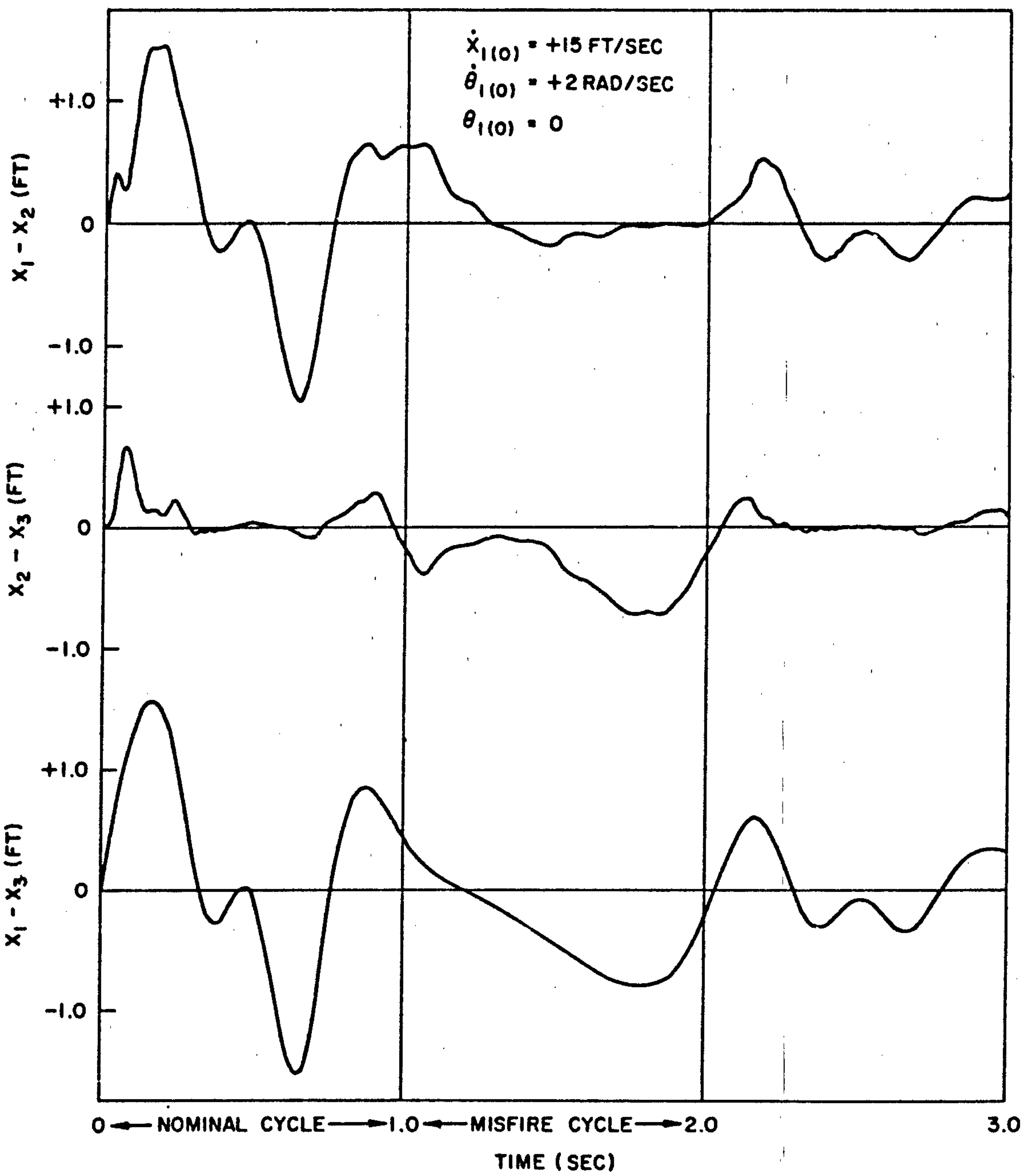

Fig. 18--Combined lateral and tilting motion--with axial motion (lateral displacement)

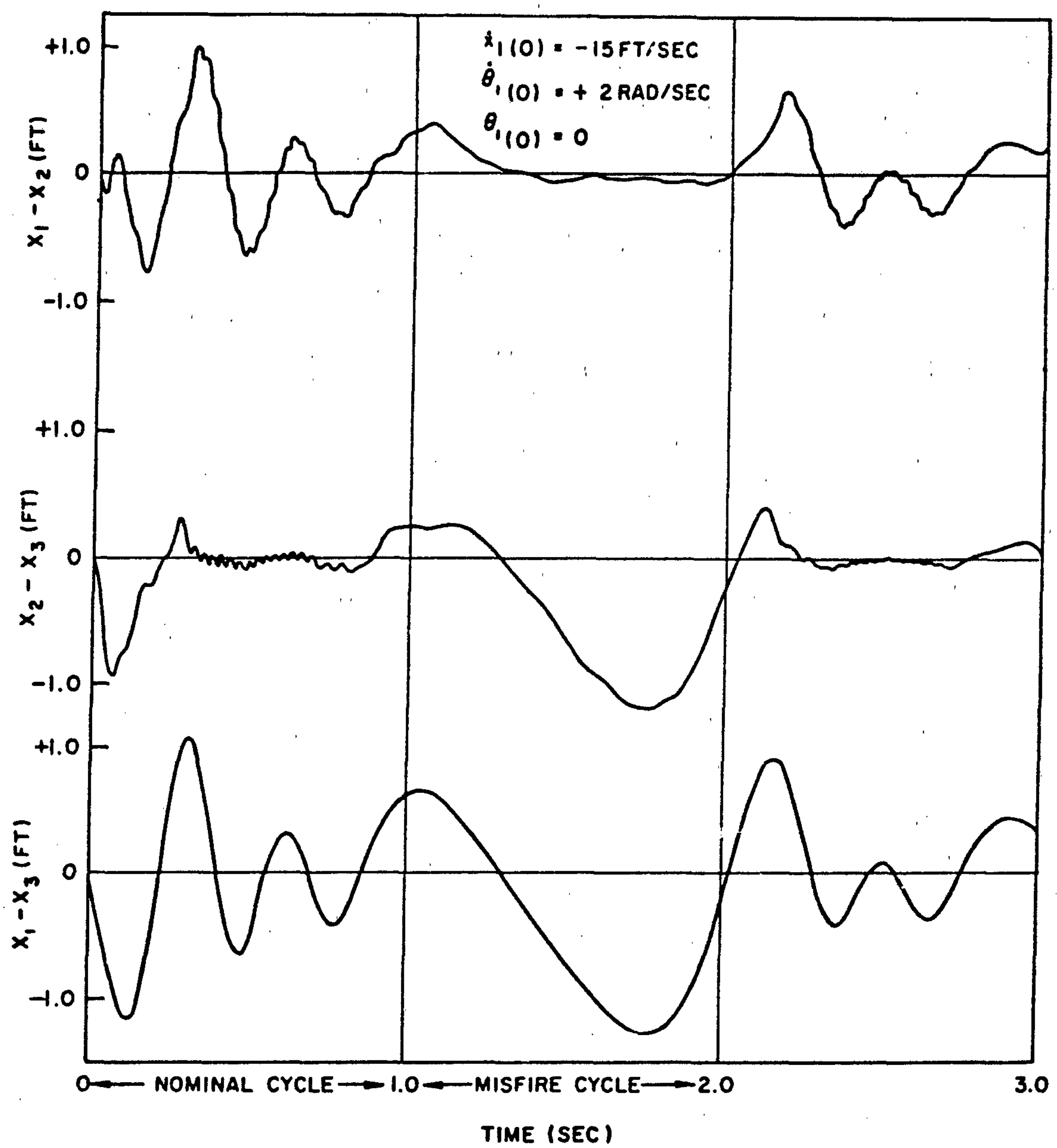

Fig. 19--Combined lateral and tilting motion--with axial motion (lateral displacement)

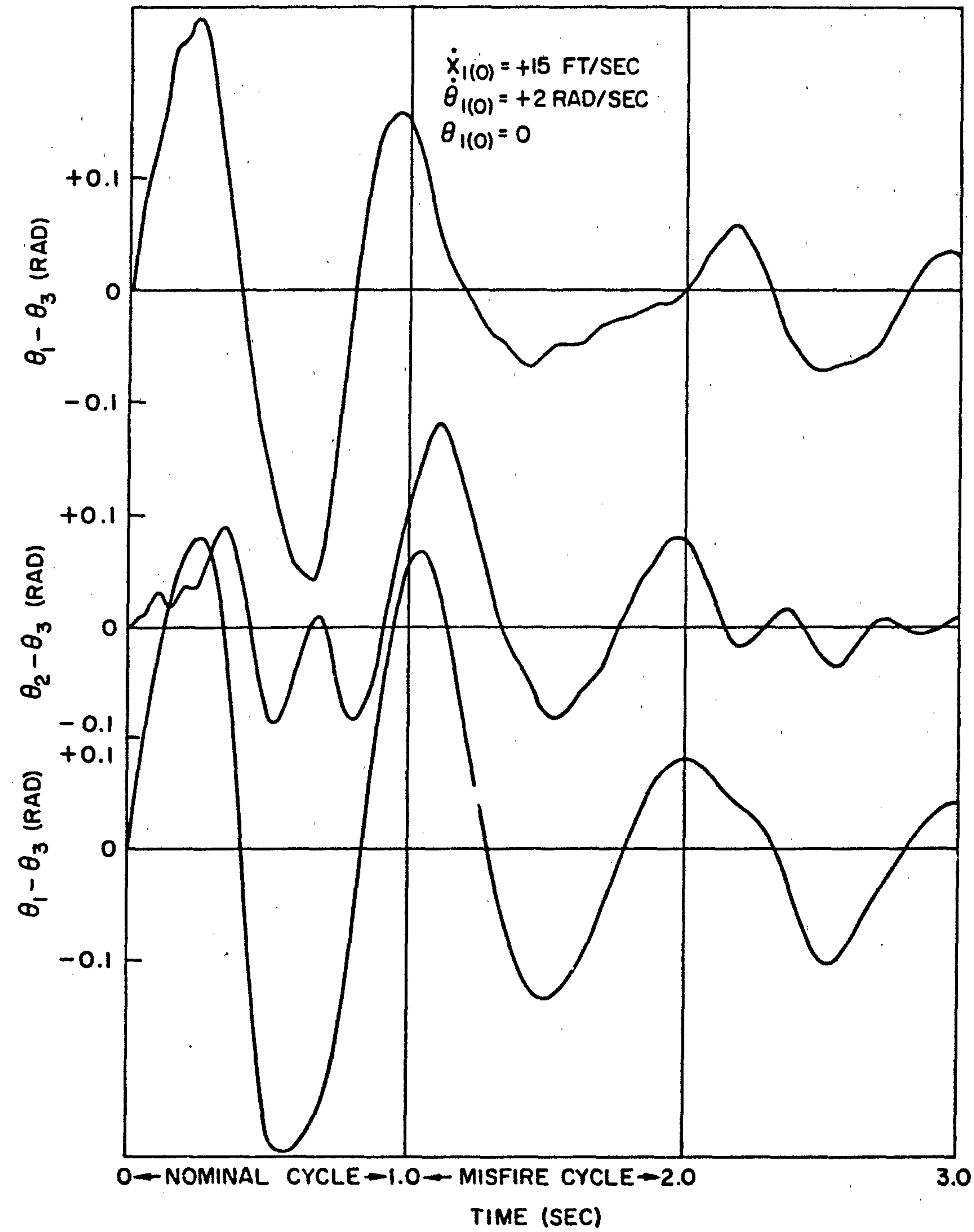

Fig. 20--Combined lateral and tilting motion--with axial motion (angular displacement)

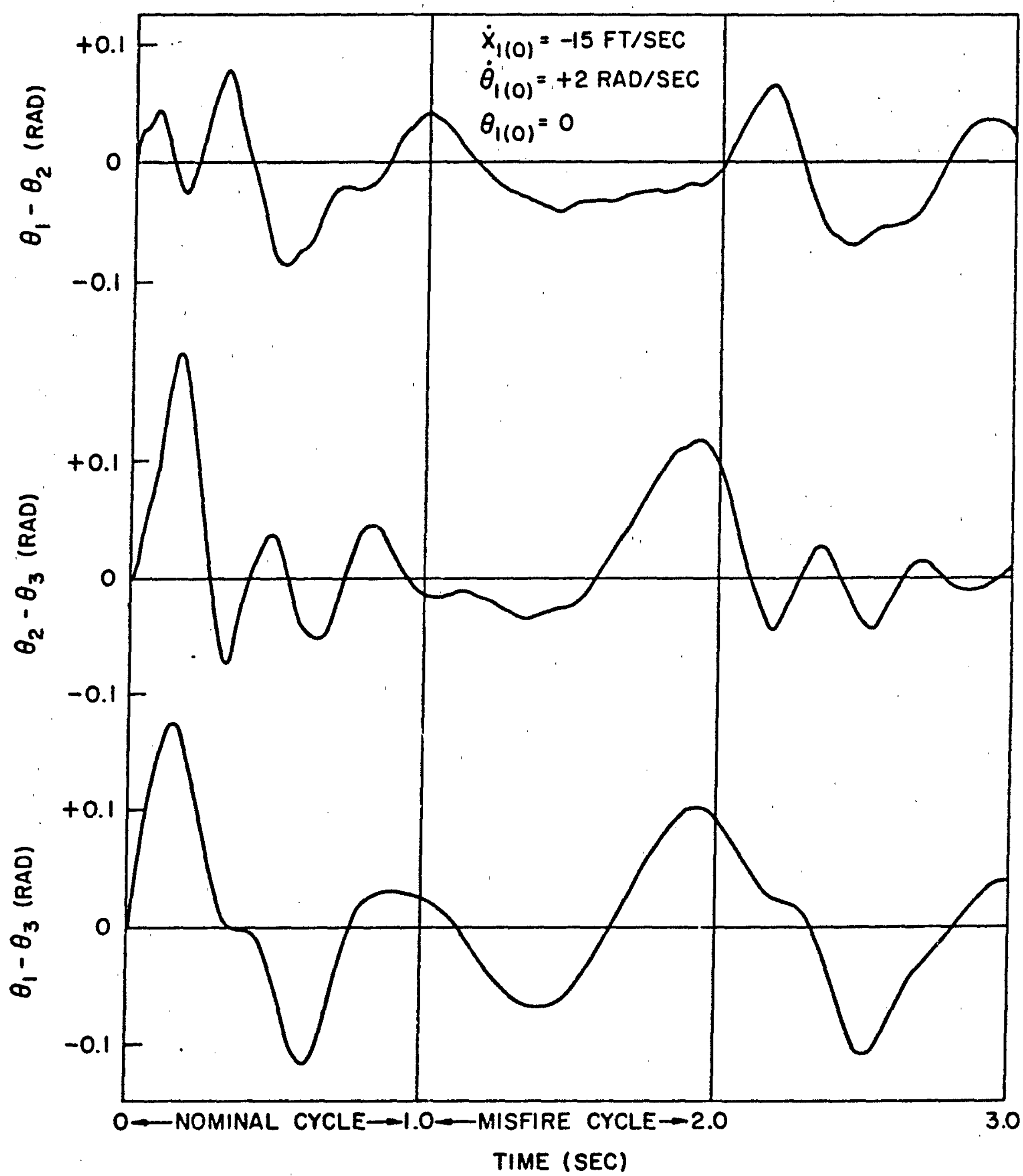

Fig. 21--Combined lateral and tilting motion--with axial motion (angular displacement)

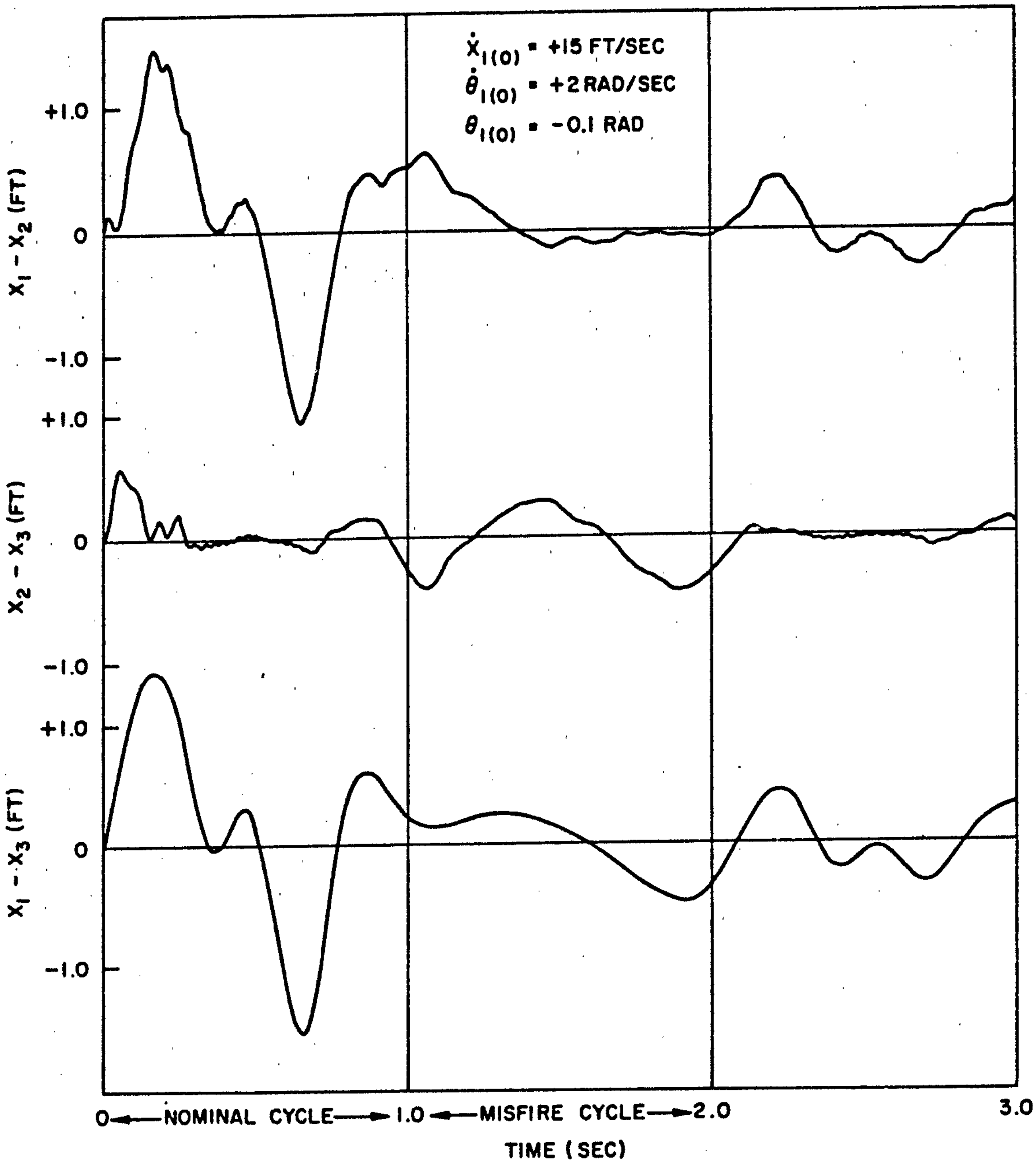

Fig. 22--Combined lateral and tilting motion--with axial motion (lateral displacement)

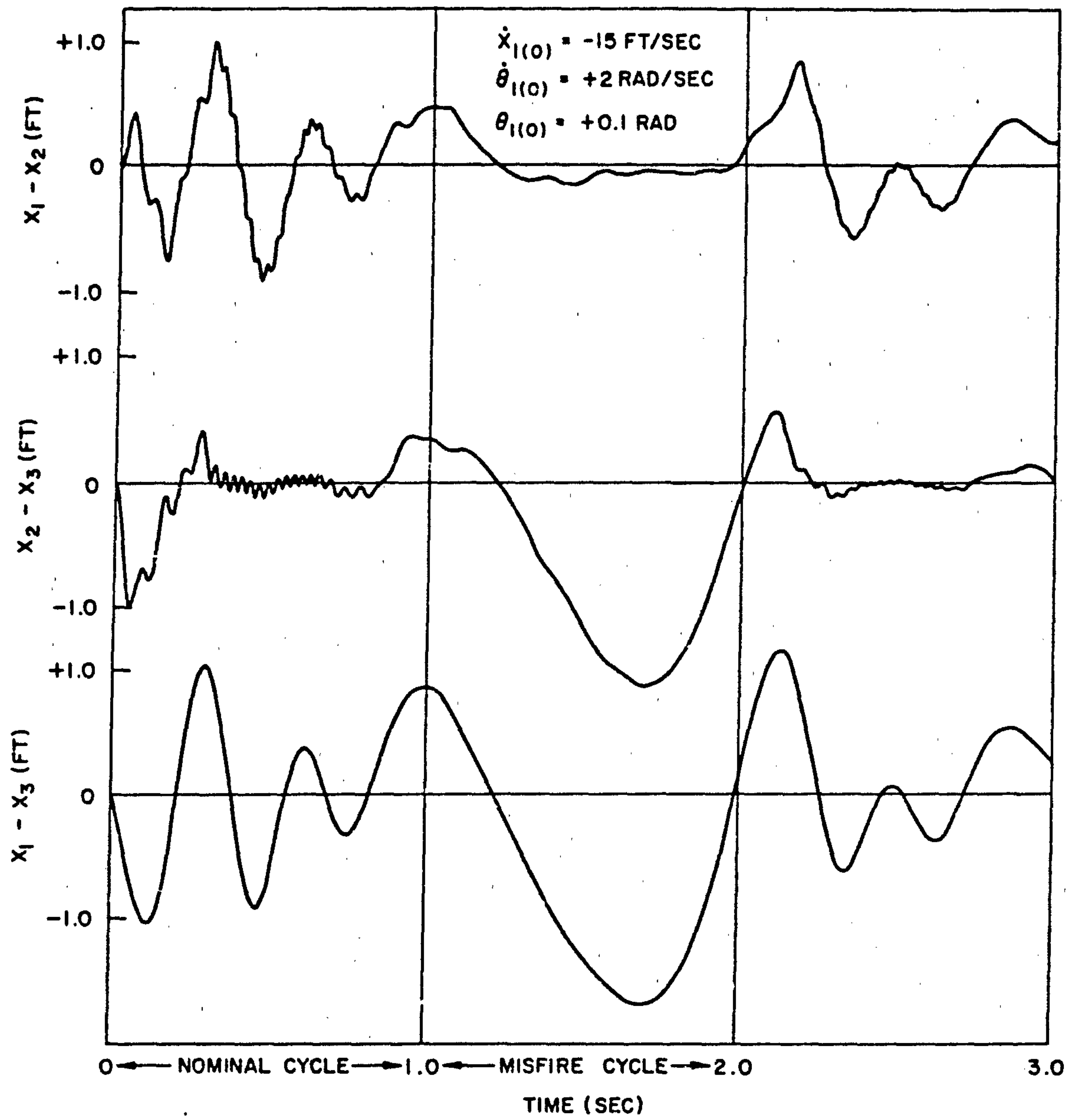

Fig. 23--Combined lateral and tilting motion--with axial motion (lateral displacement)

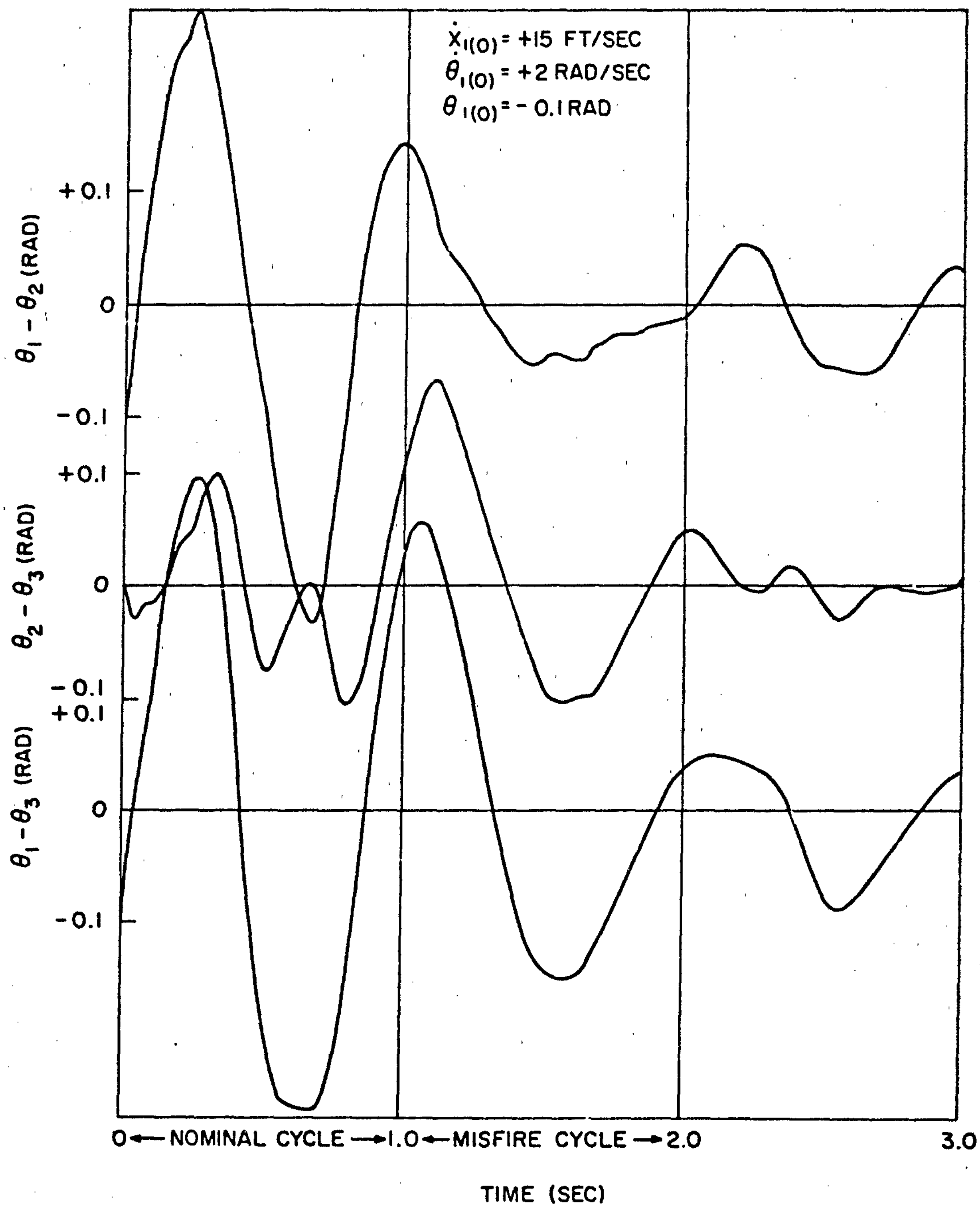

Fig. 24--Combined lateral and tilting motion--with axial motion (angular displacement)

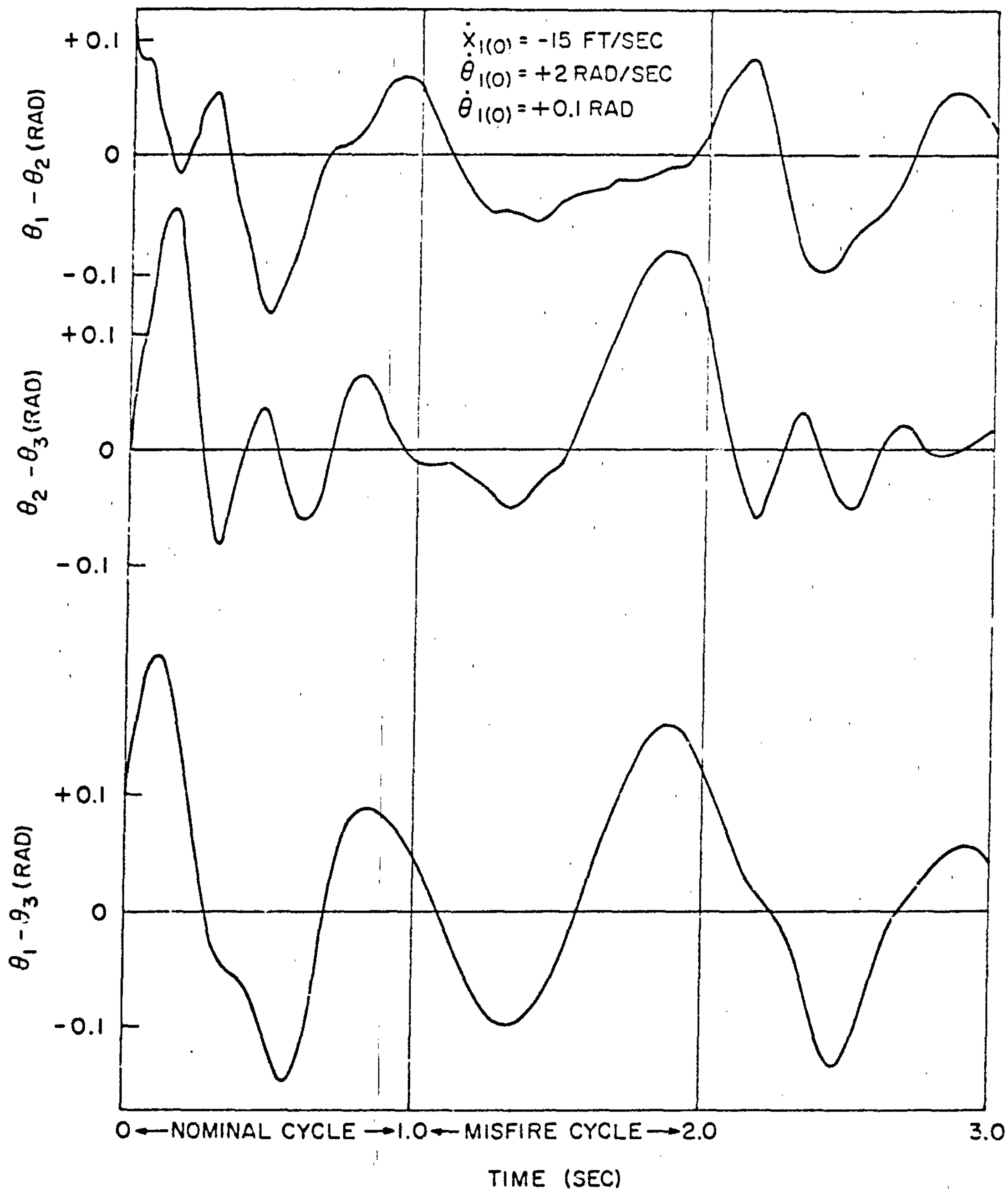

Fig. 25--Combined lateral and tilting motion--with axial motion (angular displacement)

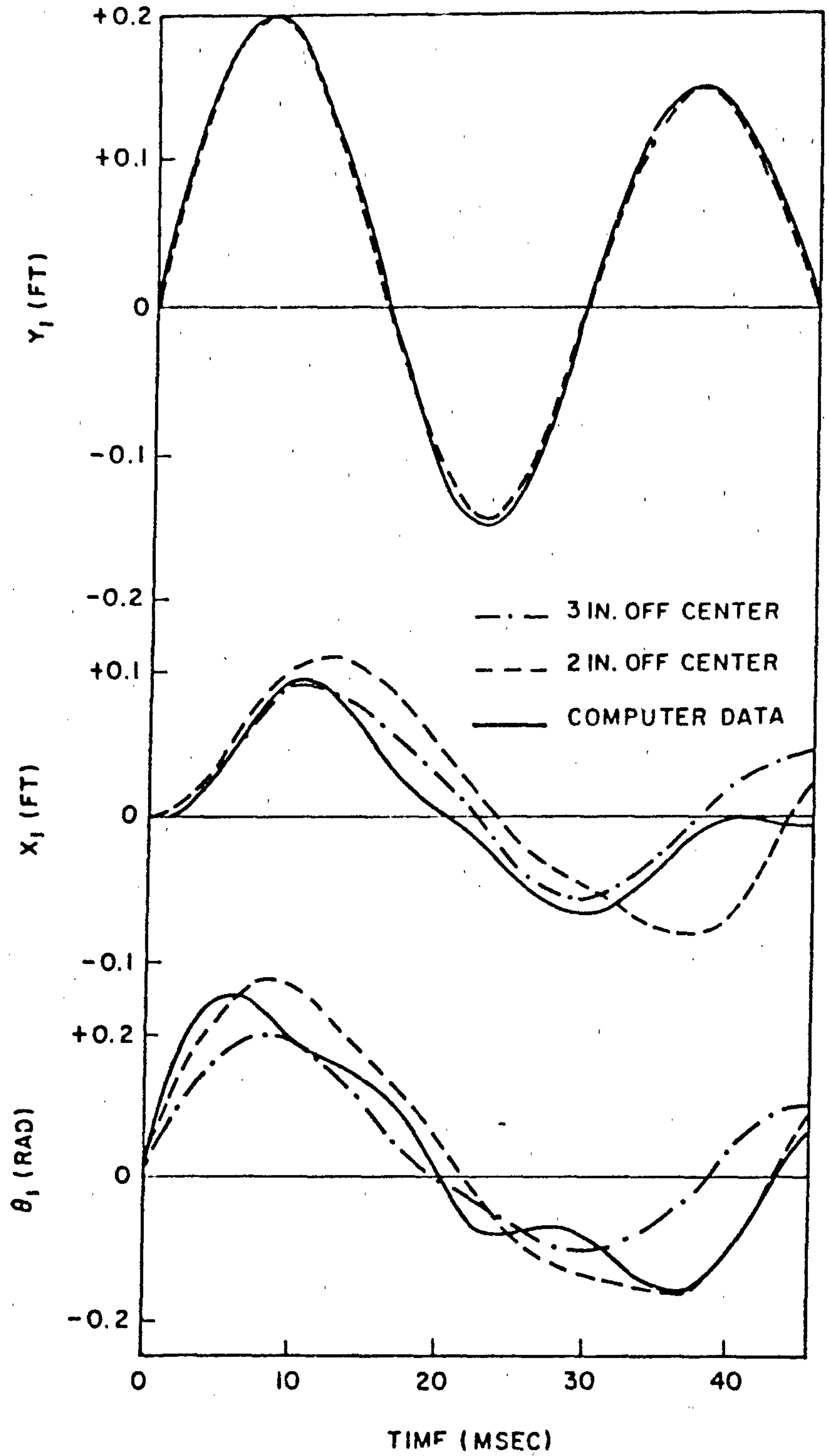

Fig. 26--Typical matching of experimental results with analog computer simulation

V. DISCUSSION

Since it was not possible to determine with certainty whether or not the system would be stable with the sequenced random impulse application outlined in Section 2, an attempt was made to estimate the likelihood of stability by the following method. The values of the various displacements and velocities of the two lower masses with respect to the upper mass in the lateral and tilting motion modes at the end of a normal cycle were compared with the values they were given at the start of the same cycle. This comparison, for both magnitude and sign, then indicated whether a positive or negative feedback was present in the system and permitted an estimate of its gain. The amount of damping in the system could also be evaluated. The initial values of $\Theta_{1(0)}$, $x_{1(0)}$, $\dot{\Theta}_{1(0)}$, and $\dot{x}_{1(0)}$ at time t = 0 were chosen so that they were compatible in magnitude and sign. Equations (42), (43), (46), (47), (48), (49), (50), (51), and (52) were used to that effect. Realistic values of Δx_e and $\Delta\Theta_e$ were chosen from the curves of Fig. 3. After several trial and error calculations, the following values were adopted for all runs:

$$\dot{\Theta}_{1(0)} = +2 \text{ rad/sec},$$
$$\dot{x}_{1(0)} = \pm 15 \text{ ft/sec},$$
$$\Theta_{1(0)} = \mp 0.1 \text{ rad},$$
$$x_{1(0)} = 0 \text{ (for simplification sake)}.$$

For the sign conventions used (see Fig. 1) and according to Eq. (43), only the following two combinations are possible:

$$\dot{x}_{1(0)} > 0 \quad \text{for } \Theta_{1(0)} < 0,$$
$$\dot{x}_{1(0)} < 0 \quad \text{for } \Theta_{1(0)} > 0.$$

For all these runs, the system was always given the nominal impulse in the longitudinal direction. Since there was no feedback between the lateral and tilting-motion modes and the longitudinal-motion mode, the on-axis oscillations repeated exactly for all initial conditions investigated. The longitudinal oscillations, on the contrary, strongly affected the lateral and tilting motions of the intermediate mass and, to lesser extent, those of the lower mass.

The curves of Figs. 18 through 25 were analyzed and the results obtained are given in Tables 3 and 4. It seems that for both $\Theta_{1(0)} = 0$ and $\Theta_{1(0)} \neq 0$, the lateral motion of the pusher plate is damped out appreciably at the end of a nominal cycle especially, for $\Theta_{1(0)} = 0$. The tilting motion of the pusher plate is also damped, but the magnitude of the angular displacement of the plate is larger at the end of a cycle than it is at the beginning for $\dot{x}_{1(0)} > 0$ and $\dot{\Theta}_{1(0)} > 0$. An ideally placed explosion at the end of this cycle would therefore tend to amplify the lateral oscillation of the pusher plate but since the plate is off-centered in the positive direction, part of the plate tilting momentum would be canceled, which would provide a stabilizing effect. But it is impossible to evaluate this effect quantitatively at this time.

It is therefore quite difficult to predict whether the nominal system first investigated would be stable under normal operating conditions.

The cause of the difficulty is the cross-coupling between the tilting-motion and lateral-motion modes. It so happens that the reactions due to $\dot{x}_{1(0)}$ and $\dot{\Theta}_{1(0)}$ add when of opposite sign. Two simple and practical solutions are available to alter this cross-coupling:

1. Increase the lateral and angular stiffnesses of the second spring, and
2. Increase the damping in the first spring in the lateral-motion and tilting-motion modes, especially in the tilting-motion mode.

Both of these were tried and they yielded the following results: An increase of 50% in the stiffness of the second spring for both the lateral restoring force and the moment reaction does not change the response of the

Table 3

INITIAL AND FINAL CONDITIONS FOR A NOMINAL CYCLE, $\theta_{1(0)} = 0$

Parameter	Initial Conditions $x_{1(0)} = x_{2(0)} = x_{3(0)} = 0$ $\theta_{1(0)} = \theta_{2(0)} = \theta_{3(0)} = 0$	Final Conditions $\dot{x}_{1(0)} > 0,\ \dot{\theta}_{1(0)} > 0$	Final Conditions $\dot{x}_{1(0)} < 0,\ \dot{\theta}_{1(0)} > 0$
$(x_1 - x_2)$, ft	C	+0.9	+0.30
$(x_1 - x_3)$, ft	0	+0.7	0
$(\dot{x}_1 - \dot{x}_3)$, ft/sec	+15 and -15	+3.5	-11
$(\dot{x}_2 - \dot{x}_3)$, ft/sec	0	+2.0	-10
$(\theta_1 - \theta_2)$, rad	0	+0.25	+0.10
$(\theta_1 - \theta_3)$, rad	0	+0.27	+0.08
$(\dot{\theta}_1 - \dot{\theta}_3)$, rad/sec	+2	-0.9	-0.47
$(\dot{\theta}_2 - \dot{\theta}_3)$, rad/sec	0	+0.15	+0.50

Table 4

INITIAL AND FINAL CONDITIONS FOR A NOMINAL CYCLE, $\theta_{1(0)} = \pm 0.1$ rad

Parameter	Initial Conditions	Final Conditions	
	$x_{1(0)} = x_{2(0)} = x_{3(0)} = 0$ $\theta_{2(0)} = \theta_{3(0)} = 0$	$\dot{x}_{1(0)} > 0,\ \dot{\theta}_{1(0)} > 0$ $(\theta_{1(0)} < 0)$	$\dot{x}_{1(0)} < 0,\ \dot{\theta}_{1(0)} > 0$ $(\theta_{1(0)} > 0)$
$(x_1 - x_2)$, ft	0	+1.0	+0.2
$(x_1 - x_3)$, ft	0	+0.80	0
$(\dot{x}_1 - \dot{x}_3)$, ft/sec	+15 and -15	+5.5	-13
$(\dot{x}_2 - \dot{x}_3)$, ft/sec	0	+0.2	-10
$(\theta_1 - \theta_2)$, rad	-0.1 and +0.1	+0.26	+0.08
$(\theta_1 - \theta_3)$, rad	-0.1 and +0.1	+0.27	+0.07
$(\dot{\theta}_1 - \dot{\theta}_3)$, rad/sec	+2	0	-0.9
$(\dot{\theta}_2 - \dot{\theta}_3)$, rad/sec	0	+0.1	+0.6

system to an appreciable degree, as shown by a comparison of the results presented in Table 5 with those of Tables 3 and 4. But the high-frequency lateral oscillations of the intermediate platform are less pronounced. Of course, the amplitudes of the lateral- and tilting-motion mode oscillations of the intermediate platform are decreased appreciably; this effect, although small, is useful.

The increase in damping of the first spring in the lateral- and tilting-motion modes by a factor of 2 does not improve the results appreciably either; although if the tilting-motion-mode damping is increased again by a factor of 2.5, the improvement is substantial and would make the system definitely stable. This is quite obvious, as illustrated by the results of Tables 6 and 7. There is no doubt that such a large amount of damping might be difficult to provide; nevertheless, it is not out of the question that a damping rate increase between the two factors 2 and 5 might be achievable and sufficient to ensure stability.

The influence of the change in stiffness of the second spring during a compression and especially during a misfire cycle is very pronounced. For instance, the high-frequency vibration of the $(x_2 - x_3)$ curves of Figs. 19 and 24 are caused by the rigidity of the second spring when compressed. These vibrations disappear as soon as the intermediate platform comes back through its neutral position. The two lower masses thus behave as a unique mass during the misfire cycle, oscillating at a low frequency until the pusher plate comes back up past its neutral position. A compression cycle starts again and the normal frequencies reappear.

In practice, the stiffness of the second spring should not increase so rapidly and the frequency of the low-amplitude high-frequency vibrations of Figs. 19 and 24 should not be as high as shown. But the actual variation of stiffness with stroke is difficult to evaluate accurately. Therefore, an attempt was made to vary the influence of the pusher-plate stroke on the second-spring lateral stiffness. The results were noticeable but there was no improvement in the stability of the system, as indicated by the results of Table 8. The maximum amplitudes of $(x_1 - x_3)$ and $(\theta_1 - \theta_3)$ were increased; the frequency of the intermediate platform lateral vibrations was decreased.

Table 5

INFLUENCE OF SECOND-SPRING LATERAL RIGIDITY, $(K_2$ and $K_3) \times 1.5$, ON FINAL CONDITIONS AFTER NOMINAL CYCLE

Parameter	$\theta_{1(0)} = 0$		$\theta_{1(0)} \neq 0$	
	$\dot{x}_{1(0)} > 0$ $\dot{\theta}_{1(0)} > 0$	$\dot{x}_{1(0)} < 0$ $\dot{\theta}_{1(0)} > 0$	$\dot{x}_{1(0)} > 0$ $\dot{\theta}_{1(0)} > 0$	$\dot{x}_{1(0)} < 0$ $\dot{\theta}_{1(0)} > 0$
$(x_1 - x_2)$, ft	+0.85	+0.4	+0.2	+1
$(x_1 - x_3)$, ft	+0.70	0	-0.3	+0.95
$(\dot{x}_1 - \dot{x}_3)$, ft/sec	+6	-10	-8	+7
$(\dot{x}_2 - \dot{x}_3)$, ft/sec	+1.5	-3	-4.5	+5
$(\theta_1 - \theta_2)$, rad	+0.25	+0.14	+0.16	+0.24
$(\theta_1 - \theta_3)$, rad	+0.26	+0.16	+0.18	+0.25
$(\dot{\theta}_1 - \dot{\theta}_3)$, rad/sec	-0.6	-0.8	-0.7	-0.20
$(\dot{\theta}_2 - \dot{\theta}_3)$, rad/sec	0	+0.55	+0.7	0

Table 6

INFLUENCE OF FIRST-SPRING DAMPING, $r_1 \times 2$, $q_1 \times 2$, ON FINAL CONDITIONS AFTER NOMINAL CYCLE

Parameter	$\theta_{1(0)} = 0$		$\theta_{1(0)} \neq 0$	
	$\dot{x}_{1(0)} > 0$, $\dot{\theta}_{1(0)} > 0$	$\dot{x}_{1(0)} < 0$, $\dot{\theta}_{1(0)} > 0$	$\dot{x}_{1(0)} > 0$, $\dot{\theta}_{1(0)} > 0$	$\dot{x}_{1(0)} < 0$, $\dot{\theta}_{1(0)} > 0$
$(x_1 - x_2)$, ft	+0.6	+0.5	+0.6	+0.3
$(x_1 - x_3)$, ft	+0.35	+0.6	+0.45	+0.1
$(\dot{x}_1 - \dot{x}_3)$, ft/sec	+2.0	-9.0	+4	-10.5
$(\dot{x}_2 - \dot{x}_3)$, ft/sec	0	-6.0	+2	-6
$(\theta_1 - \theta_2)$, rad	+0.16	+0.11	+0.16	+0.10
$(\theta_1 - \theta_3)$, rad	+0.17	+0.065	+0.17	+0.07
$(\dot{\theta}_1 - \dot{\theta}_3)$, rad/sec	-0.7	0	-0.4	-0.3
$(\dot{\theta}_2 - \dot{\theta}_3)$, rad/sec	+0.1	+0.3	0	+0.5

Table 7

INFLUENCE OF FIRST-SPRING DAMPING, $r_1 \times 2$, $q_1 \times 5$,
ON FINAL CONDITIONS AFTER NOMINAL CYCLE

Parameter	$\theta_{1(0)} = 0$		$\theta_{1(0)} \neq 0$	
	$\dot{x}_{1(0)} > 0$ $\dot{\theta}_{1(0)} > 0$	$\dot{x}_{1(0)} < 0$ $\dot{\theta}_{1(0)} > 0$	$\dot{x}_{1(0)} > 0$ $\dot{\theta}_{1(0)} > 0$	$\dot{x}_{1(0)} < 0$ $\dot{\theta}_{1(0)} > 0$
$(x_1 - x_2)$, ft	+0.25	+0.25	+0.20	+0.20
$(x_1 - x_3)$, ft	0	+0.30	+0.10	+0.15
$(\dot{x}_1 - \dot{x}_3)$, ft/sec	+3.0	-7.0	+3.5	-1.0
$(\dot{x}_2 - \dot{x}_3)$, ft/sec	+1.0	-4.5	+1.5	-7.0
$(\theta_1 - \theta_2)$, rad	+0.06	+0.07	+0.07	+0.08
$(\theta_1 - \theta_3)$, rad	+0.08	-0.03	+0.08	+0.05
$(\dot{\theta}_1 - \dot{\theta}_3)$, rad/sec	-0.03	0	0	-0.2
$(\dot{\theta}_2 - \dot{\theta}_3)$, rad/sec	0	0	0	0

Table 8

INFLUENCE OF SECOND-SPRING LENGTH, L_0 = 22 FT,
ON FINAL CONDITIONS AFTER NOMINAL CYCLE

Parameter	$\theta_{1(0)} = 0$		$\theta_{1(0)} \neq 0$	
	$\dot{x}_{1(0)} > 0$ $\dot{\theta}_{1(0)} > 0$	$\dot{x}_{1(0)} < 0$ $\dot{\theta}_{1(0)} > 0$	$\dot{x}_{1(0)} > 0$ $\dot{\theta}_{1(0)} > 0$	$\dot{x}_{1(0)} < 0$ $\dot{\theta}_{1(0)} > 0$
$(x_1 - x_2)$, ft	+1.1	+0.25	+1.1	+0.15
$(x_1 - x_3)$, ft	+1.15	+1.15	+1.2	+1.0
$(\dot{x}_1 - \dot{x}_3)$, ft/sec	-5.5	-4.2	-2.5	+8
$(\dot{x}_2 - \dot{x}_3)$, ft/sec	-1.5	+7.0	0	-8
$(\theta_1 - \theta_2)$, rad	+0.235	0	+0.24	-0.01
$(\theta_1 - \theta_3)$, rad	+0.18	-0.09	+0.21	-0.11
$(\dot{\theta}_1 - \dot{\theta}_3)$, rad/sec	-1.4	-0.30	-1.0	-0.35
$(\dot{\theta}_2 - \dot{\theta}_3)$, rad/sec	+0.15	-0.25	+0.2	0

The influence of the clearance between the pistons and the cylinders of the second-stage shock-absorber system was also studied. An increase of the clearance should have a destabilizing effect, but not a pronounced one as long as the radial clearance does not exceed 1/4 in. This is borne out by the results given in Table 9.

Finally, the cross-coupling effects between the tilting and lateral motions of mass M_1, as illustrated by the curves of Figs. 12 and 13, although large, agree with the results obtained several years ago[9] when an experimental 3-torus-stack shock absorber was dynamically tested with an HE-driven plate. A comparison between the experimental results reported in Ref. 9 and the results given by the analog computer yielded the curves of Fig. 26. The matching of the analog computer runs with the experimental results are excellent for the axial-motion mode. The agreement is less satisfactory for the lateral- and tilting-motion modes, although the frequencies, cross-coupling effects, and general shape of the curves match within the accuracy achievable with the test-data reduction techniques available.[9]

VI. CONCLUSIONS AND RECOMMENDATIONS

As the complete problem could not be programmed and investigated under the present contract, the stability of the engine operation could not be proven definitely. Nevertheless, sufficient results were obtained for single-impulse application to give good indications that the system is probably stable under normal operating conditions provided some improvements are made to the system, such as the amount of damping in the tilting-motion mode of the torus system.

Although a fair amount of work remains to be done to complete this investigation, the following tangible results have been secured:

1. The on-axis motion stability of the system determined with digital computer techniques was verified with the analog computer for several sequenced impulses. It appears that the tolerances given in Ref. 4 are correct.

2. The application of a single impulse, both off-centered and misoriented, was studied for the first time. The results

~~SECRET~~

Table 9

INFLUENCE OF SECOND-SPRING BACKLASH, $t_1 \times 10$,
ON FINAL CONDITIONS AFTER NOMINAL CYCLE

Parameter	$\theta_{1(0)} = 0$		$\theta_{1(0)} \neq 0$	
	$\dot{x}_{1(0)} > 0$, $\dot{\theta}_{1(0)} > 0$	$\dot{x}_{1(0)} < 0$, $\dot{\theta}_{1(0)} > 0$	$\dot{x}_{1(0)} > 0$, $\dot{\theta}_{1(0)} > 0$	$\dot{x}_{1(0)} < 0$, $\dot{\theta}_{1(0)} > 0$
$(x_1 - x_2)$, ft	+0.95	+0.27	+1.0	+0.30
$(x_1 - x_3)$, ft	+0.68	-0.10	+0.8	0
$(\dot{x}_1 - \dot{x}_3)$, ft/sec	+3.2	-10	+5.5	-13
$(\dot{x}_2 - \dot{x}_3)$, ft/sec	-1.7	-10	+0.15	-9
$(\theta_1 - \theta_2)$, rad	+0.25	+0.11	+0.26	+0.065
$(\theta_1 - \theta_3)$, rad	+0.27	+0.08	+0.27	+0.06
$(\dot{\theta}_1 - \dot{\theta}_3)$, rad/sec	-0.9	-0.37	0	-0.9
$(\dot{\theta}_2 - \dot{\theta}_3)$, rad/sec	+0.14	+0.52	0	+0.6

~~SECRET~~

showed that the pusher-plate and intermediate-platform oscillations are either sufficiently damped out or out of phase (negative feedback) at the end of any single firing cycle so that the application of a new off-centered or misoriented impulse would probably not lead to increasing amplitudes of these oscillations.

3. The lateral rigidity of both shock-absorber stages is adequate, at least during the normal compression cycle.

4. The only factor that could be increased practically and that has an appreciable influence on the system stability is the first-spring damping in the tilting-motion mode. This damping should be made as large as possible.

5. Appreciable variation of some of the most significant variables do not alter the system stability appreciably.

6. Only the complete stability study as outlined in Section 2 can give positive information on the system stability.

7. The mathematical model derived from the structural analysis of the torus system is accurate and flexible enough to allow fair simulation of actual test data during a full 1 1/2-cycle excursion in the axial-motion mode. Therefore, one can have confidence in the results obtained with the engine model used on the analog computer, although some coefficients might have to be adjusted to fit better experimental data when available.

8. The damping coefficients required to fit the mathematical model of the torus system with the experimental data for the lateral- and tilting-motion modes were considerably larger than those adopted for the engine simulation runs. Therefore, it seems that the increase by a factor of 5 of the torus-system damping coefficient in the tilting-motion mode, recommended as a means to increase stability, is quite realistic.

Since the sidewise impulse is proportional to the on-axis impulse, it does not seem, as a first approximation, that the impulse magnitude per explosion would affect the stability characteristics. The engine size should also be immaterial. The major dependency is the ratio of the stiffnesses of the springs in the lateral direction as compared to that in the longitudinal direction. For the engine-model configuration selected, this factor should not vary appreciably and therefore the single investigation of any realistic model should be sufficient at the present time. The masses of the pusher plate and intermediate platform cannot be changed appreciably, and since they dictate the frequency ratios between the various modes of oscillations for a given mass, very little can be done here. But one could consider a different frequency ratio between spring 1 and spring 2, for instance, 7:1 or 11:1 instead of 9:1 as is currently used (see Refs. 3 and 4). This might affect the system behavior appreciably.

The present study should be continued so that the stability of the ORION vehicle can be established for at least two configurations--a vehicle fully loaded (corresponding to the mission departure gross weight) and an empty vehicle (weight after mission completion)--under normal operating conditions (repeated sequenced impulses chosen at random).

Stabilizing influences such as the longitudinal spinning of the vehicle should be studied at a later date. This should prove to be a very significant factor for two reasons: It would reduce the amplitude of all tilting oscillations for a given explosion off-centering because of gyroscopic effects, and it could also be used to transform positive feedback either of the θ or x, or both, into negative feedback, which would tend to stabilize an inherently unstable system. This could be achieved by spinning the vehicle at a rate of $(2n + 1)\pi/\tau$ rps, where n is an integer (0, 1, 2, 3, ...) and τ is the nominal firing period.

Appendix A

SECOND-SPRING LATERAL STIFFNESS

The second spring of the system consists essentially of six thin-walled circular beams of variable length. These beams are the second-stage shock-absorber pistons, and they are clamped at both ends to connect the intermediate platform to the upper vehicle.(4) These piston stems are much more flexible than the cylinders in which they are guided and thus they are assumed to be the only deformable structure. The deflection of a beam of constant cross section when subjected to a concentrated load at one end, if no tilting of the clamped end is allowed (which is almost the case for the present application), is

$$f = \frac{WL^3}{3EI},$$

where f = deflection,

W = load,

L = length between the clamped ends,

E = modulus of elasticity of the material,

I = cross-section moment of inertia.

If one end is fully articulated, the beam is much more flexible and

$$f = \frac{WL^3}{48EI},$$

or the beam is 16 times less rigid.

A very comprehensive analysis of this problem is presented in Ref. 7, and if one writes

$$f = K\frac{WL^3}{EI},$$

it is possible to determine K so that the present case agrees fairly well with the most logical case examined in Ref. 7. Taking $E = 16 \times 16^6$ psi (for titanium) and the piston-wall dimensions given in Ref. 3,

$$f = \frac{WL^3}{K_3},$$

where $K_3 = 5 \times 10^8$ per piston, then for six pistons one has

$$W = 3 \times 10^9 \, fL^{-3};$$

but since

$$W = F(x_2 - x_3),$$

$$f = x_2 - x_3,$$

$$L = L_0 - [(y_{3,00} - y_{2,00}) - (y_3 - y_2)]$$

and if L_0 is the free length of the piston in the neutral position, one finally has

$$F(x_2 - x_3) = 3 \times 10^9 \{L_0 - [(y_{3,00} - y_{2,00}) - (y_3 - y_2)]\}^{-3} (x_2 - x_3).$$

The introduction of the effect of the clearance between the pistons and the cylinders in this equation yields Eq. (26); $(y_{3,00} - y_{2,00}) - (y_3 - y_2)$ is the intermediate-platform travel with respect to the upper vehicle.

Appendix B

SECOND-SPRING RESTORING MOMENT

The tilting of the unclamped end of a beam of constant cross section that is clamped at the other end is given by

$$\Delta\theta = \tan^{-1} \int_0^{x=L} \frac{M\,dx}{EI} = \tan^{-1}\left(\frac{ML}{EI}\right).$$

Therefore, ignoring the fact that all six piston stems cannot have the same length when the intermediate platform tilts, one has

$$ML = K_2 \tan \Delta\theta$$

or, finally, $$M(\theta_3-\theta_2) = K_2 \tan \Delta\theta\, L^{-1},$$

where L is as given in Appendix A and $K_2 = 2.5 \times 10^8$ for the configuration studied. Although it was tacitly assumed in Appendix A that the lateral displacement of the intermediate platform could not cause any tilting, one must consider the influence of any lateral displacement on the curvature of the piston stem. It can be additive or subtractive. The sketch of Fig. 27 illustrates this quite well.

According to the sign convention of Fig. 1, a positive lateral displacement $+x_2$ creates an increase of the bending moment caused by a tilting angle $-\Delta\theta_2$. As a first approximation, one can show that the increase $\delta\theta$ of $\Delta\theta_2$ due to the $+x_2$ displacement is

$$\delta\theta = \frac{2x_2}{\ell}$$

or for the configuration investigated,

$$\delta\theta = \frac{2(x_2 - x_3)}{L_0 - [(y_{3,00} - y_{2,00}) - (y_3 - y_2)]} \cdot$$

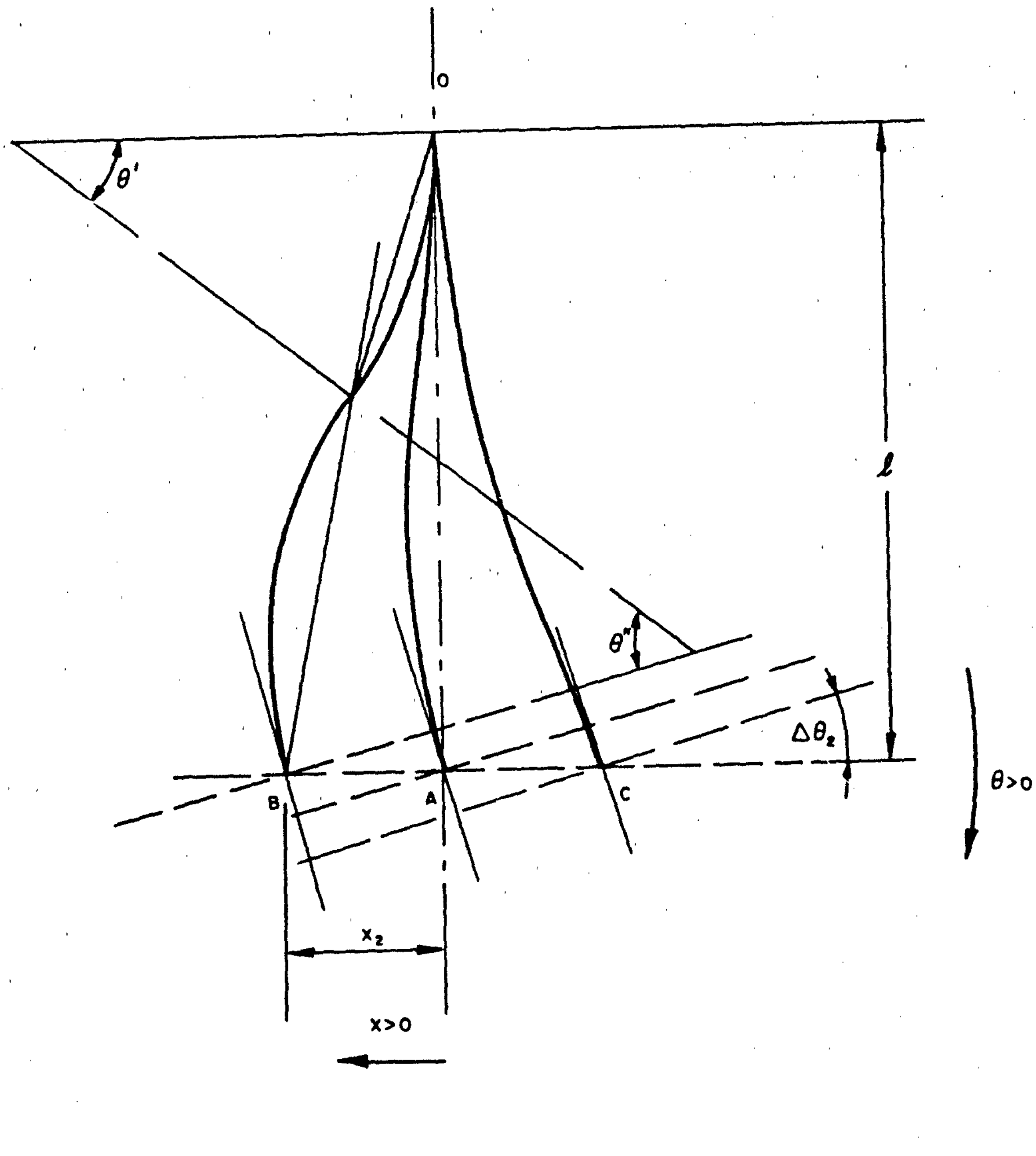

Fig. 27--Influence of the lateral motion of mass M_2 on the deformation of spring 2

Therefore, the moment reacting on the intermediate platform is caused by an equivalent angle

$$\Delta\theta = -\Delta\theta_2 - \delta\theta$$

or, more generally,

$$\Delta\theta = (\theta_2 - \theta_3) - \frac{2(x_2 - x_3)}{L_0 - [(y_{3,00} - y_{2,00}) - (y_3 - y_2)]} \cdot$$

Appendix C

FUNCTIONS GENERATED BY DFG'S FOR THE ENGINE SIMULATION AND THE EXPERIMENTAL TORUS SYSTEM

Figures 28 through 33 present the curves generated by the diode function generators (DFG's) for the engine simulation.

The functions $g(\alpha)$, $j(\alpha)$, $h(\beta)$, and $1/2\ell(\alpha)$ for the experimental torus-system simulation are tabulated in Table 10.

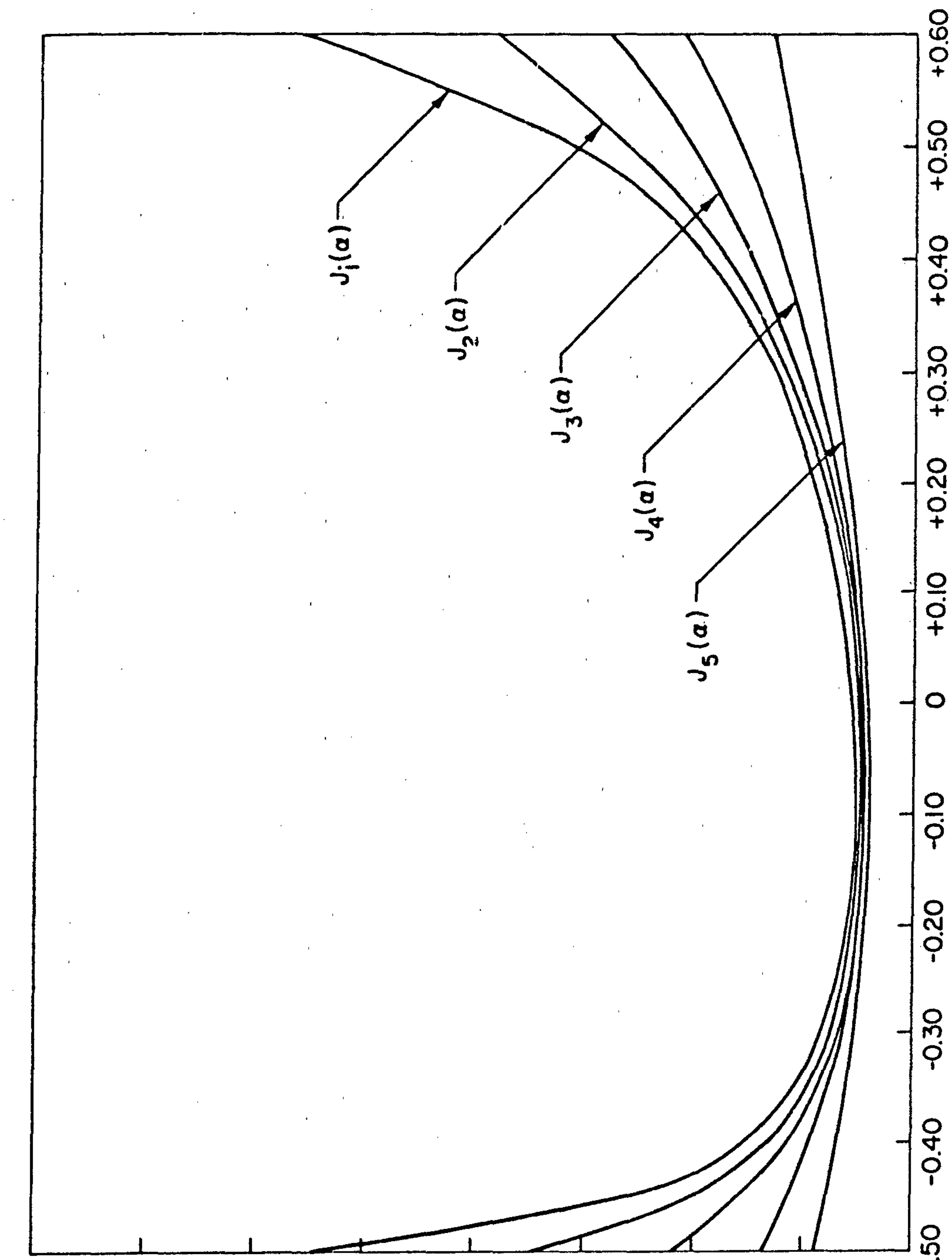

Fig. 28--Functions $J_i(\alpha)$ - DFG' No. 1 to 5

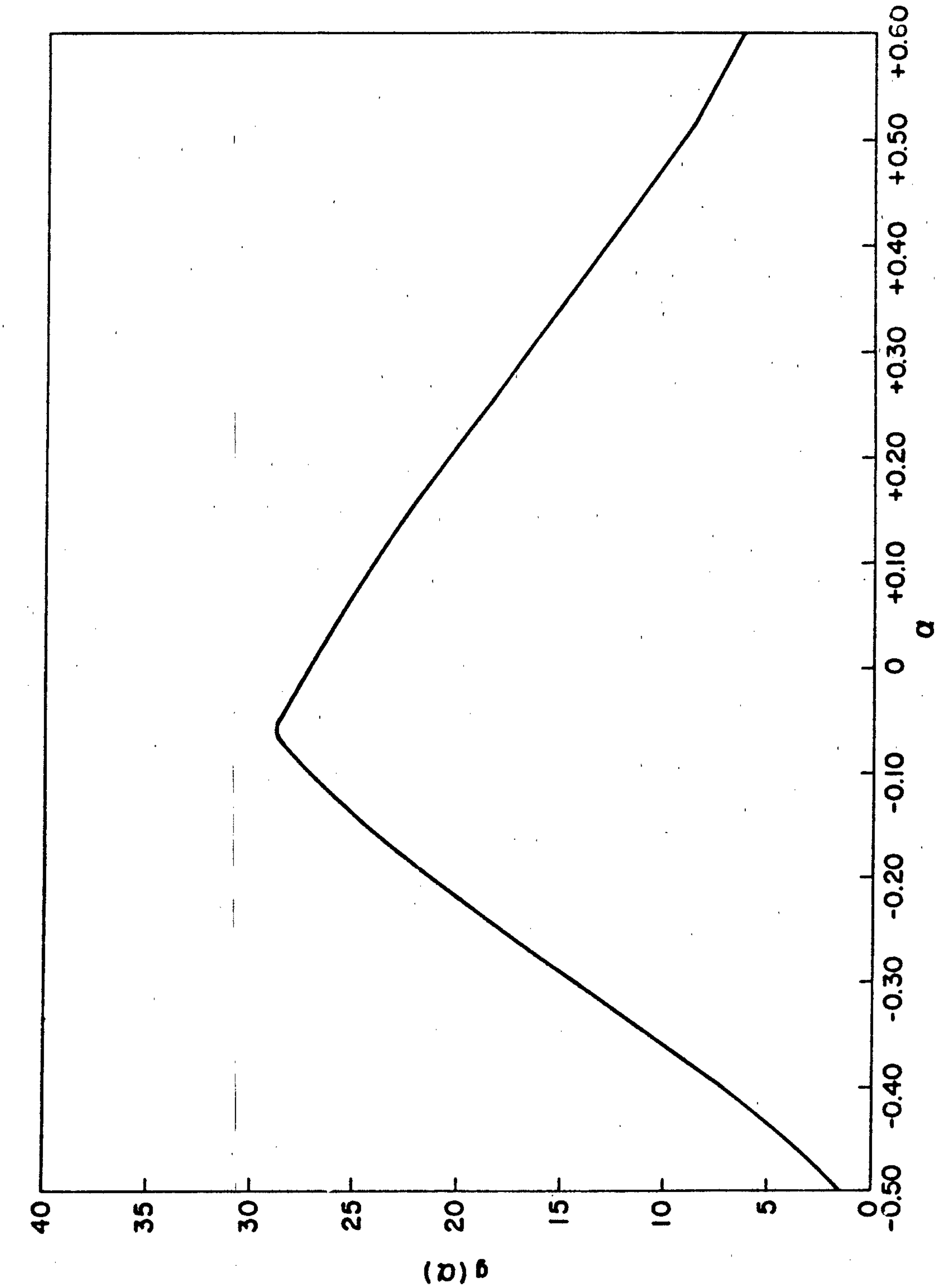

Fig. 29--Function g(α) - DFG No. 6

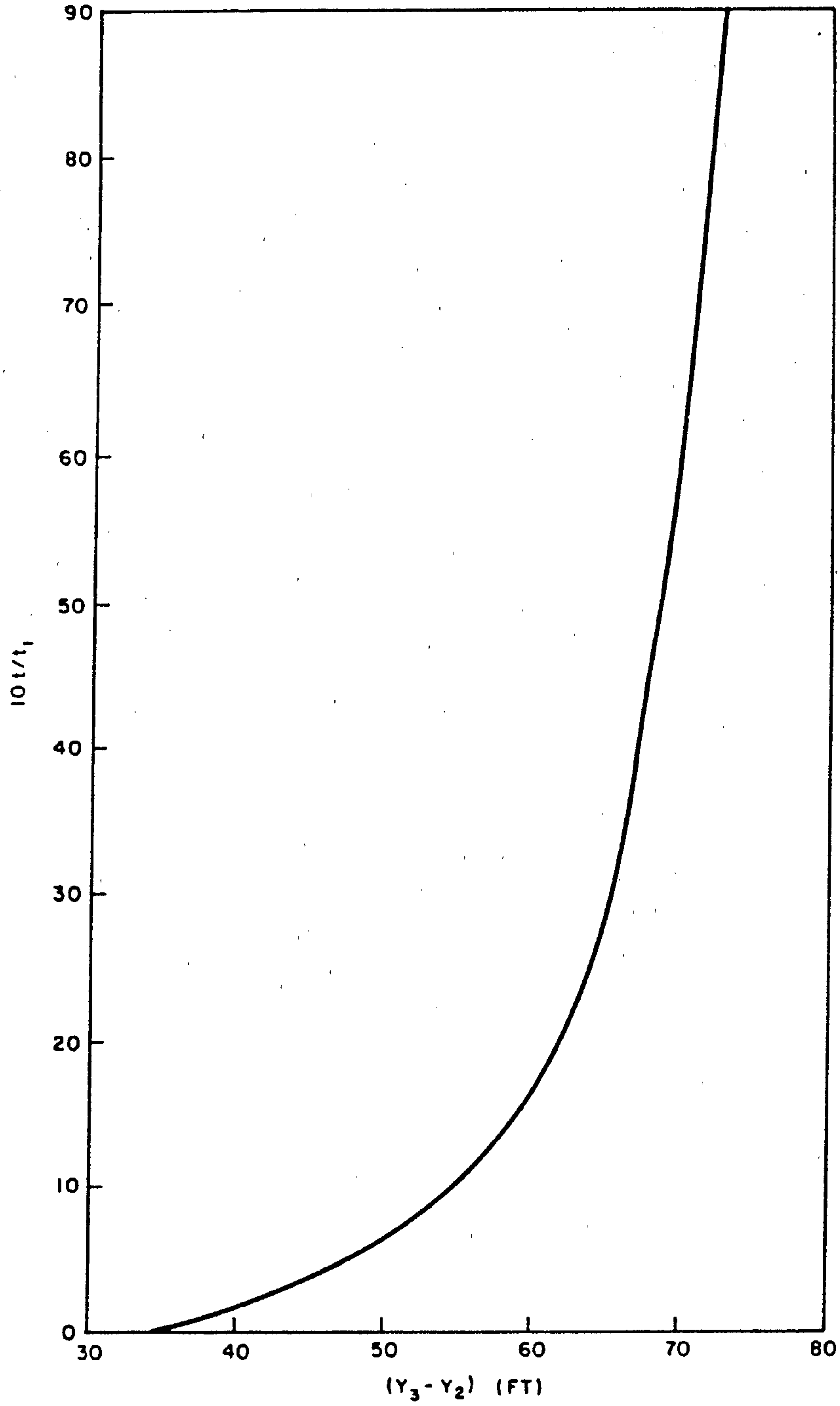

Fig. 30--Function $10t/t_1$ - DFG No. 7

UNCLASSIFIED

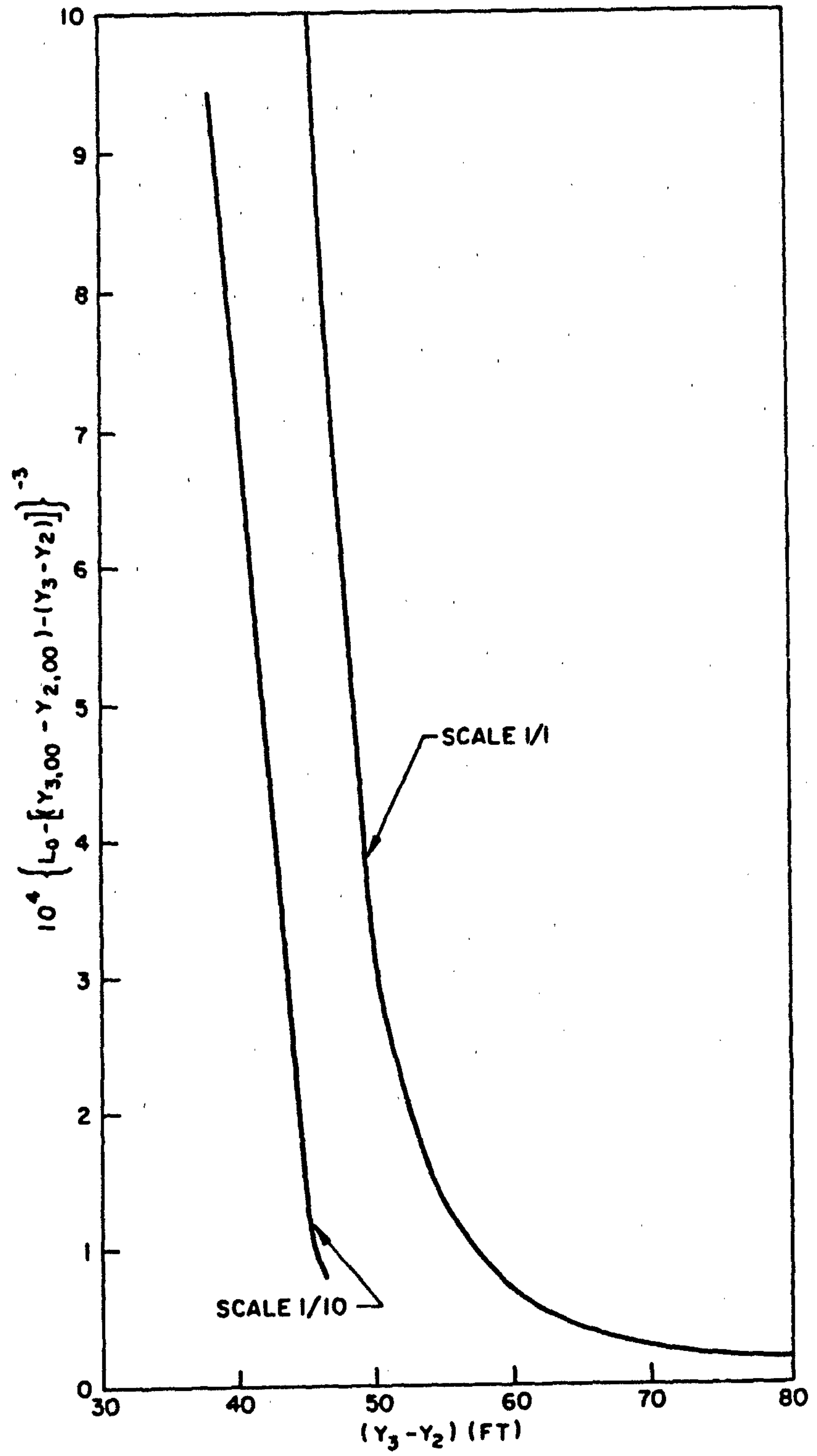

Fig. 31--Function $10^4\{L_0 - [(y_{3,00} - y_{2,00}) - (y_3 - y_2)]\}^{-3}$ - DFG No. 8

UNCLASSIFIED

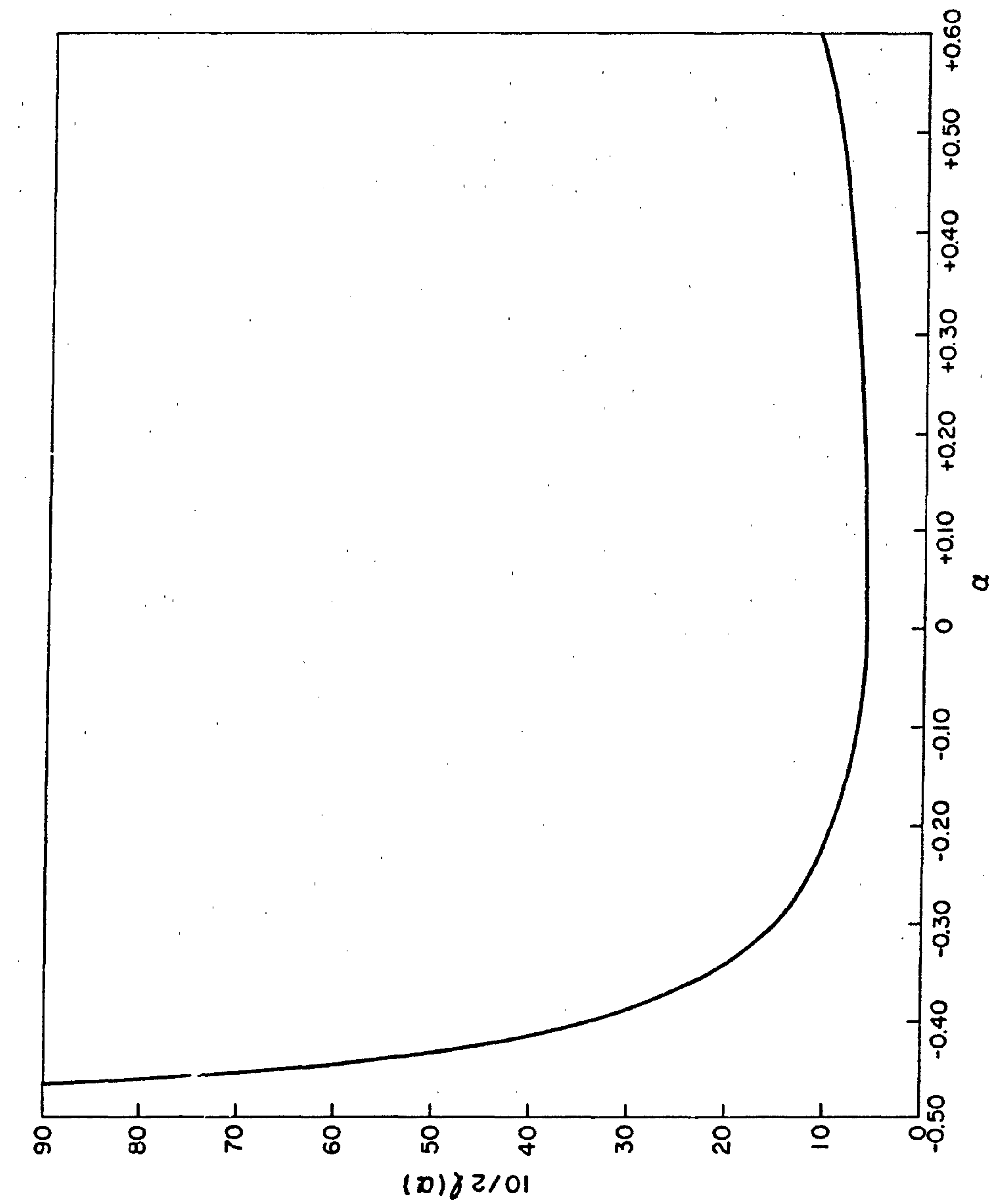

ig 32--Function 10/2 $\ell(\alpha)$ - DFG No. 9

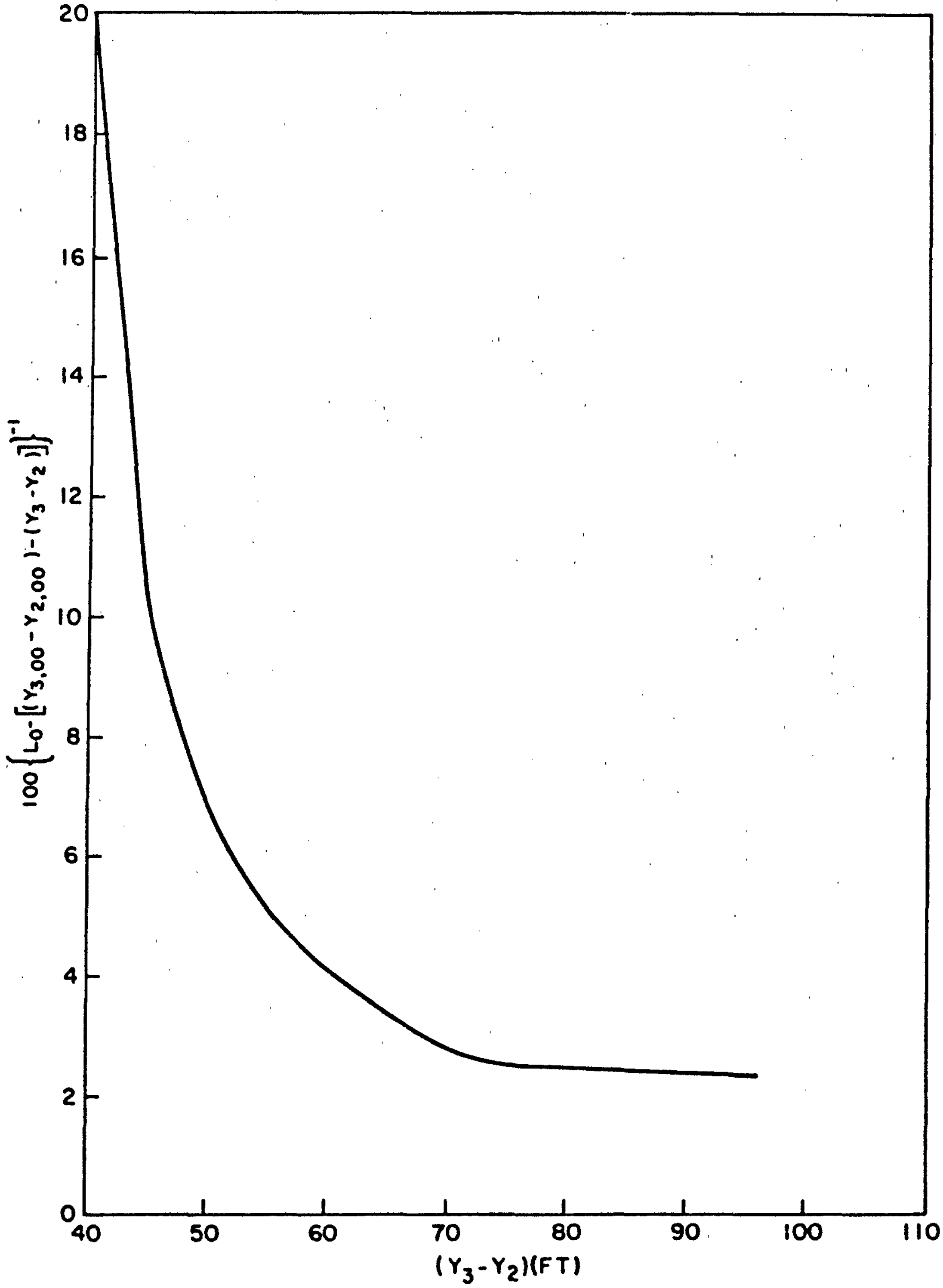

Fig. 33--Function $100\left\{L_0 - \left[(y_{3,00} - y_{2,00}) - (y_3 - y_2)\right]\right\}^{-1}$ - DFG No. 10

Table 10

EXPERIMENTAL TORUS SYSTEM SIMULATION

FOR $g(\alpha)$, $j(\alpha)$, $h(\beta)$, AND $1/2\ell(\alpha)$

α	$g(\alpha)$	$h(\beta)$	$j(\alpha)$	$1/2\ell(\alpha)$
-0.5	0.01493	0.02560	29.52	16.739
-0.45	0.04031	0.02093	23.51	5.995
-0.40	0.07283	0.01871	17.73	3.203
-0.35	0.1089	0.01740	13.94	2.066
-0.30	0.1458	0.01656	11.54	1.486
-0.25	0.1819	0.01598	9.995	1.145
-0.20	0.2155	0.01556	8.994	0.9278
-0.15	0.2461	0.01525	8.340	0.7786
-0.10	0.2731	0.01502	7.930	0.6711
-0.05	0.2962	0.01484	7.702	0.5907
0	0.2701	0.01470	8.728	0.6170
+0.05	0.2559	↓	9.561	0.6187
+0.10	0.2440		10.43	0.6249
+0.15	0.2230		11.79	0.6353
+0.20	0.2049		13.28	0.6507
+0.25	0.1862		15.07	0.6711
+0.30	0.1674		17.23	0.6970
+0.35	0.1481		19.88	0.7311
+0.40	0.1292		23.06	0.7736
+0.45	0.1107		26.87	0.8278
+0.50	0.09289		31.38	0.8969
+0.60	0.06051		95.97	1.101

[redacted]

UNCLASSIFIED

Appendix D

TABLE OF CONSTANTS AND EQUATION COEFFICIENTS

FOR ENGINE SIMULATION

Masses (slugs)

$M_1 = 3180$

$M_2 = 415$

$M_3 = 27{,}300$

Moments of Inertia (slugs x ft^2)

$I_1 = 1.4 \times 10^5$

$I_2 = 1.4 \times 10^4$

$I_3 = 1.12 \times 10^7$

Damping Coefficients

$p_1 = 500$	$p_2 = 150$
$q_1 = 1.4 \times 10$	$q_2 = 10^4$
$r_1 = 2500$	$r_2 = 1635$

Forces and Moments

$A = 3.36 \times 10^5$	$k_1' = 1300$	$D_1 = 5.5$ ft
$B = 2.75 \times 10^5$	$k_2'' = 435$	$D_2 = 10.5$ ft
$c = 1.1 \times 10^4$	$K_2 = 2.5 \times 10^8$	$D_3 = 16$ ft
$S = 1$	$K_3 = 3 \times 10^9$	$D_4 = 21$ ft
		$D_5 = 29$ ft

UNCLASSIFIED

[redacted]

Initial Conditions

$y_{1,00} = 0$ $\quad$ $y_{2,00} = 8$ ft $\quad$ $y_{3,00} = 63$ ft

$\dot{y}_{1(0)} = 63$ ft/sec

Engine-configuration Geometry

$L_0 = 20$ to 22 ft $\quad$ $r_g = 6.64$ ft

$t_1 = 2 \times 10^{-3}$ ft $\quad$ $\lambda_0 = 30$ ft

Appendix E

CALCULATIONS OF EXPERIMENTAL TORUS-SYSTEM SPRING CONSTANT

The dimensions of the experimental 3-ton torus system were

Diameter = 11.8 in. $\cong$ 1 ft,

Height = 5.17 in. $\cong$ 0.43 ft.

The plate characteristics were:

Weight = $\sim$ 8 lb,
Mass, m_1 = 0.25 slugs,
Moment of Inertia = 0.0212 slug $\times$ ft^2,
Radius of Gyration = 0.291 ft.

The plate was given an initial axial velocity of 38 to 42 ft/sec with the impulses off-centered from 0.5 in. to 3.5 in. This produced initial angular velocities, $\dot{\theta}_{1(0)}$, of 40 to $\sim$ 120 rad/sec.

From static compression and tension test data,(9) the value of k_1' (or K_1, as used in Table 2) was $\sim$ 1500. In Eqs. (10) and (11), the value of A was in the vicinity of 1000.

In the axial direction, for displacements of the order of 0.2 ft, the plate oscillating frequency was between 35 and 40 cps.(9)

The best match between the simulated curves and the experimental results given in Fig. 26 was obtained for values of A and k_1' that differed from the calculated values as follows:

A was adjusted to 1150 instead of 1000,

k_1' for $F_{(x)}$ was adjusted to 550 instead of 1500,

k_1' for $M(\theta)$ was adjusted to between 1000 and 1200 instead of 1500.

Although the adjustment required for A was small, the adjustment of k_1' is large, especially for the lateral-motion-mode coefficient. No satisfactory explanation has been found, except that this experimental system was far from ideal and that it cannot be ascertained that no lateral initial velocity increment was given to the plate at the time of the explosion.

REFERENCES

1. The Nuclear/Chemical Pulse Reaction Propulsion Project (Project ORION)--Summary Report (U), General Atomic Report GA-2419, July 18, 1961. (Secret/RD report)

2. Technical Summary Report, Nuclear-pulse Propulsion Project (Project ORION) (U), Vol. I--Reference Vehicle Design Study, RTD-TDR-63-3006, October 1963. (Secret/RD report)

3. Technical Summary Report, Nuclear-pulse Propulsion Project (Project ORION) (U), Vol. III--Engine Design, Analysis, and Development Techniques, WL-TDR-64-93, December, 1964. (Secret/RD report)

4. David, C. V., et al., Double-stage Shock Absorber Investigati (U), General Atomic, Informal Report GAMD-5911, December, 1964. ecret report)

5. Ross, F. W., Stability of Motion Induced by Blast (U), General Atomic, Informal Report GAMD-937, August 18, 1958. (Secret report)

6. David, C. V., Axial and Lateral Rigidity of Pressurized Toroidal Filament Structures, General Atomic, Informal Report GAMD-6061, January 13, 1965. (Unclassified)

7. Boden, O. W., Review of Intermediate Platform, Secondary Shock-absorber Piston-tube Materials and Fabrication Problems (U), General Atomic, Informal Report GAMD-5408, June 17, 1964. (Secret report)

8. Teichmann, T., The 'ngular Effects Due to Asymmetric Placement of Axial Symmetric Explosives, General Atomic, Informal Report GAMD-5823, October 26, 1964. (Unclassified)

9. David, C. V., Toroidal Shock-absorber Scale-model Testing (14-in. Pusher Plate) (S), Inner-tube Spring Assembly Test (U), General Atomic, Informal Report GAMD-2554, October 5, 1961. (Secret report)